

Analytical and Experimental Study of X-ray Absorption Coefficients of Material by Abel's Inversion*

S. J. Han

P.O. Box 4684, Los Alamos, NM 87544-4684

email:sjhan@cybermesa.com

Abstract

The hard x-ray (γ -ray) absorption by cylindrically symmetric U^{238} test objects is studied by means of γ -ray transmission measurements. To make a precise comparison between the theoretically modelled values and the absorption coefficients calculated from the experimental data, we have developed a highly accurate numerical code based on a new solution of Abel's integral equation. It is shown that progressive filtering, surface reflections by Compton scattering, and the enhanced backscattering due to impurities can explain much of the observed discrepancy. We also discuss optimal experimental conditions with regard to the feasibility of quantitative radiography for γ -ray diagnostics.

PACS numbers:

* This study was performed for DAHRT project by the author at LANL (LA-UR-91-1966) and was supported by DOE.

I. INTRODUCTION

The calculation of precise radial density profiles for a localized radiation source (*i.e.*, soft x-ray emission by hot plasmas) has been a long standing problem in both plasma physics and astrophysics [1, 2, 3, 4, 5]. For a sufficiently tenuous plasma in which radiation emission processes dominate over absorption processes, the symmetric density profile of the plasma can be obtained from the projected radiation intensity by Abel's inversion.

Another example of the application of Abel's inversion is the determination of density profiles of an imploding spherical targets driven by laser-beams [6]. These two seemingly different diagnostic methods are mathematically identical and rely on the solutions of Abel's integral equation [1, 2, 3, 4, 5].

Before proceeding further, it is important to point out that there have been extensive studies on the absorption of a soft x-ray by the Abel's integral equation for medical applications by Cormack [9] who apparently was not aware of previous work on the x-ray diagnostics employed in Astrophysics [1, 2, 3, 4, 5]. Despite numerous studies over many years [7], there still exists considerable debate over the importance of a numerical method for solving the integral equation. The numerical algorithm by Barr [8] has attracted considerable interest, particularly with the observation of a diffuse background due to Compton scattering.

In all x-ray diagnostics, the x-rays are normally produced by a high-energy electron accelerator and depend on the bremsstrahlung process in a high Z-material. In particular, the PHERMEX electron accelerator at Los Alamos that is a 50 MHz, 30 MeV standing-wave device which operates at 500 A with 600 kV injector. It has been relatively a simple task to focus the high current electron beam by injecting a neutral plasma by means of self-focusing by a self- pinching mechanism [10] and thus creates a point-like high energy x-ray (or γ -ray) source. The x-rays are produced by the scattering of the high-energy electron beam at a target material (usually high Z-material such as tungsten). The electrons lose their energy by two basic process: collision and radiation. The collision process leaves the atoms in the material either excited states or the ionized states. The ejected electrons have a small energy that is deposited locally. On the other hand the x-rays (radiation energy) generated by bremsstrahlung process is uniformly distributed among secondary photons of all energies up to the energy of the primary electron energy itself.

At the energy of PHERMEX electron beam, the bremsstrahlung process dominates over

the collision process. For an optimal radiography, it is essential to have a pencil beam to create a point source of the x-rays at a distance far from the test object. This provides approximately a parallel x-ray beam as shown in Figure 1. Moreover, the spot size of a point source determines the spatial resolution in an X-ray film.

This optimal condition allows one to study a density profile of a test object by means of Abel's integral equation [19]. In all previous numerical calculations based on the Volterra solution of Abel integral equation [1], expressing the data as a well-behaved function was an essential step to avoid the noise amplification. When the data, which contain small random errors due to a photon cascade and large fluctuations by the enhanced backscattering at the impurities, are smoothed by polynomial fits, the calculations tend to obscure the basic processes. Moreover, the smoothing leads to a hybridization of random errors and fluctuations such that the computed absorption coefficients do not provide any meaningful information about absorption coefficients. Worse yet, the results are often misleading.

Here we report a study, by flash x-ray photography, of the absorption coefficients of metallic cylinders of high Z -material (U^{238}) with a high concentration of impurities. First we discuss a new numerical solution to Abel's integral equation and its application to a cylindrically symmetric object using experimental data. We then discuss the results, their relevance, and connection to other work. Last we discuss optimal experimental conditions with regard to feasibility of x-ray radiography as a quantitative tool for x-ray diagnostics.

X-ray absorptions at the surface of condensed matter in photon energies below 40 KeV has been extensively studied. Experimental measurements of the absorption coefficients are in good agreement with detailed theoretical analysis [12]. However, the hard x-ray absorption mechanism at the surface has not been fully explored. We show, by specific examples, that since Compton scattering and pair production are two competing processes in x-ray absorption in the photon energy up to 5 MeV [15, 17, 20], where the upper limit of the photon energy depends on the Z -number (the cross-section of pair-production becomes equal to that of Compton scattering at 5 MeV for Pb; it is 15 MeV for Al), Compton scattering leads to a partial reflection of x-rays at a sharp boundary with a curvature. Furthermore, we show that since the basic x-ray transmission equation remains correct to the single-scattering approximation, the mean free-path of an incident photon in a given material must be sufficiently large to neglect the effect of multiple scattering.

A solid cylinder with different holes in size at both ends is ideally suited for studying

the effect of a partial reflection of x-rays at a sharp boundary on the absorption coefficients. A single exposure of an x-ray beam to the cylinder provides a data for a solid cylinder as well as for a cylinder with a void. Moreover, the circular curvature allows one to study the angular dependence of scattered photons at the surface, where the scattering centers are located.

An analytic solution to Abel's integral equation that is least sensitive to local random errors is the starting point of our study. We show, by an analytic method, that Abel's integral equation admits a different form of a solution than that obtained by Volterra [1]. This modified form of a solution not only reduces the computing time by an order of magnitude, but also allows one to analyze the effect of intensity fluctuations on the absorption coefficients.

First we review the basic x-ray absorption processes in a high- Z metallic test object and discuss the relative importance of the processes at a given energy of an x-ray. Next we review Abel's integral equation and derive its solutions in Sec. III. We then study numerical methods of data analysis based on the new solution to Abel's integral equation in Sec. IV and compare the numerical results with the known absorption coefficients of material. The application of the numerical code is discussed in Sec. V. In Sec. VI we discuss an optimal experimental condition for x-ray diagnostics and the basic requirements of an x-ray source for the condition. Lastly in Sec. VII, the feasibility of quantitative x-ray diagnostics is discussed.

II. X-RAY ABSORPTION AND TRANSPORT IN HIGH- Z MATERIAL

Pulsed high-energy x-ray sources (*e.g.* PHERMEX) have provided a way to obtain x-ray snap shots of dynamical processes such as imploding spherical targets in an ICF program. These snap shots provide the transmitted x-ray intensity profiles with a diffuse background. In PHERMEX facility at Los Alamos, the high-energy γ -rays are produced by short pulsed high-energy electron beam. The high-energy electron beam strikes the target material in which the energy loss of the beam by bremsstrahlung is fairly uniformly distributed among the secondary photons of all energies from zero up to the energy of the primary electron itself (30 MeV), for which the bremsstrahlung process dominates over the collision loss [14].

At some electron energy, the radiation loss is equal to the collision loss. This energy

coincides with the critical energy of the material, a parameter that also plays an important role in the shower theory of Rossi [13, 14]. Thus at high-energies a large fraction of the electron energy is converted to high-energy γ -rays in the target which in turn may interact with test object. The theory of high-energy photon absorption mechanism (in the order of $\mathcal{E}_\gamma \gg 2mc^2 = 1.02 \text{ MeV}$) has been extensively studied. The basic physics is fairly easy to understand and is fully described in Refs. [13, 15, 16, 17].

Next we discuss the radiation absorption process in a test object; at high-energies, the radiation absorption by pair-production (electron-positron) dominates over Compton scattering. Hence the high-energy γ rays create an electromagnetic cascade shower. The photoelectric effect and the multiple Coulomb scattering of the secondary electrons by atoms perturb the cascade shower. This coupled with Compton scattering creates a diffuse background in a radiographic film. In a thick test object, the energy of a low-energy secondary electron in the beam is dissipated by either excitation or the ionization of atoms. We will discuss further the basic processes in the radiation absorption below.

In general, as a beam of x-rays penetrates an absorbing material, its intensity shows an exponential decay. It is because a photon in the beam is removed from its original direction of penetration by either absorption or scattering in *a single event*. Since the number of photons removed in a distance dx is proportional to the beam intensity $I(x)$, the intensity of a monochromatic beam passing through the matter of a test object must decrease exponentially and is given by

$$I(x) = I_0 \exp\left[-\int_{x_0}^x \mu(x) dx\right], \quad (1)$$

where the absorption coefficient μ represents the average number of absorption and scattering processes a single photon undergoes per cm in its path and I_0 is the beam intensity at $x = x_0$.

Neglecting the effect of multiple scattering and photon cascade, the cross-section for the primary processes (*i.e.*, photoelectric effect, Compton scattering, and pair production) by which x-rays or γ -rays are absorbed is given by the sum: $\sigma_{total} = \sigma_{photo} + Z\sigma_{Comp} + \sigma_{pair}$. The absorption coefficient can be defined as $\mu = N\sigma_{total}(cm^{-1})$, where N is the number of atoms of the absorbing matter per cubic centimeter.

III. BASIC PROCESSES IN RADIATION ABSORPTION

Briefly we now digress to summarize the salient points of the photon absorption processes in condensed matter for the application of radiography:

A. Photoelectric Effect

At Photon energies less than 0.5 MeV, x-ray interaction with the material is dominated by photo-absorption in which an x-ray photon is completely absorbed by a bound electron in atoms. Consequently the bound electron jumps from its ground state to an excited state or into the continuum; the latter process is an ionization of the atom, which is usually more probable than the excitation. The cross-section for photoelectric effect is derived first by Heitler [15]. When the photon energy is not too close to the absorption edge, the cross-section for the photo-emission of a single electron from the K shell is given by $\sigma_{photo} = \sigma_{th} 4\sqrt{2}\alpha^4 Z^5 (mc^2/\mathcal{E}_\gamma)^{7/2}$, where σ_{th} is the cross-section Thompson scattering, α the fine-structure constant, Z the atomic number, and \mathcal{E}_γ the photon energy. Thus in the region of photon energies of the order of a few KeV, the cross-section for the photoelectric effect decreases rapidly as $\mathcal{E}^{-7/2}$.

For high-energy photons, $\mathcal{E} \gg mc^2$, the cross-section for the photoelectric effect is given by $\sigma_{photo} = \sigma_{th}(3/2)\alpha^4 Z^5 (mc^2/\mathcal{E}_\gamma)$. This shows that at high-energies the cross-section decreases as $1/\mathcal{E}_\gamma$ but photoelectric effect can still contribute to x-ray absorption for high-Z material up to 5 MeV (e.g., Pb) although its effect becomes increasingly small. At Photon energies higher than 1 MeV, the cross-section for the photo-absorption becomes negligible, however, compared to that of Compton scattering.

B. Compton Scattering

Scattering of photons by free electrons plays an important role in x-ray or γ -ray absorption in condensed matter. The cross-section for Compton scattering by relativistic corrections was first derived by Klein and Nishina [16]. We note that since the binding energy of the K shell electrons in atoms is of the order of KeV, the scattering a high energy photon in MeV by a bound electron is essentially equivalent to Compton scattering by a free electron.

For a cylindrical test object, the scattering center is well defined at the surface and

the angular dependence of scattered photons by the surface can be studied by the Klein-Nishina formula. For high-energy photons, the formula shows that the angular distribution of scattered photons tends to peak in the forward direction, which agrees well with the observation.

The conservation of energy and momentum give $k/k' = 1 + (k/m)(1 - \cos\theta)$, where k and k' are the energy of the incident and scattered photons respectively, and θ the angle in the units of $\hbar = c = 1$, c the velocity of light.

If the energy of an incident photon is large compared with the rest mass of an electron, the effect of Compton scattering can be studied in two extreme cases: for a very small scattering angle, the change of photon energy is negligible, and at large scattering angles, the scattered photon energy is always of the order of mc^2 . Thus the effect of Compton scattering in this case reduces to the classical Thompson scattering and the change in the photon energy becomes negligible.

An important point to emphasize is that, at high energies, the cross-section for Compton scattering σ_{Comp} varies as $(\pi\alpha^2/km)[\ln(2k/m) + 1/2]$, where α/m is the classical electron radius and k is the energy of a photon in the units of $\hbar = c = 1$. Thus the cross-section for Compton scattering decreases with the increasing energy of an incident photon. This is precisely the reason why the penetrating power of x-rays (or γ -rays) increases with increasing energy so long as no other absorption processes are important.

C. Pair Production

In the Coulomb field of a nucleus, a high-energy photon creates an electron-positron pair (i.e., $\gamma \rightarrow e^- + e^+$). No pair production can occur if the photon energy is less than $2mc^2$ or in the absence of the nuclear Coulomb field required for the conservation of energy and momentum [16, 20, 21]. The cross-section for the pair-production increases rapidly with the photon energy and reaches an asymptotic value in the relativistic limit. If the photon energy $\mathcal{E}_\gamma \gg (mc^2/\alpha)Z^{-1/3}$, then the cross-section takes the asymptotic form: $\sigma_{pair} = (\alpha^3/m^2)Z^2[(28/9)\ln(183/Z^{1/3}) - (2/27)]$, where the effect of atomic electrons through their screening of the nuclear charge is taken into account. This limiting form shows that the cross-section increases with the square of the Z -number. We also note that, for high energy photons, most of the electrons and positrons are emitted in the forward direction.

Since both the photoelectric effect and Compton scattering decrease as the photon energy increases, the pair production is the dominant absorption mechanism for very high-energy photons. Furthermore the critical energy above which pair production dominates in photon absorption decreases with increasing Z number. For example, the cross-section for pair production becomes equal to that of Compton scattering at about 5 MeV for Pb.

In elementary quantum field theory, there is a useful, general substitution rule which is valid to arbitrary orders and which relates processes of the type, $A + B \rightarrow C + D$, to the processes $A + \bar{C} \rightarrow \bar{B} + D$, where \bar{B} denotes the antiparticle of B. This substitution rule relates Compton scattering to the annihilation of an electron-positron pair into two photons (*i.e.*, $e^- + e^+ \rightarrow 2\gamma$) [21]. In a similar manner, the pair production process in condensed matter is closely related to bremsstrahlung process by high energy electrons [14, 20].

D. Multiple Scattering and the Effect of Photon Cascades

In condensed matter, γ -rays can undergo multiple scatterings, a sequence of scattering of the incident photon by bound electrons, if the mean free path of the photon is small compared to the size of a medium, which is usually the case for high- Z material [14]. Thus the critical parameter determining the effect of multiple scattering becomes negligible if the size of a medium is less than a few times of the mean free path of a photon, which is given as $\lambda_{(mfp)} = \mu^{-1}$, where μ is the absorption coefficient at a given energy in material (*e.g.*, $\lambda_{(mfp)} = 2.13$ cm at $\mathcal{E}_\gamma = 10mc^2$ for Pb). We notice from Figure 32 of Bethe and Ashkin [17] that the absorption coefficient for any given material goes through a minimum at some energy $\mathcal{E}_{\gamma m}$ of an incident photon energy. The nature of the transmitted x-rays depends on whether the energy of an incident photon is greater or less than $\mathcal{E}_{\gamma min}$. For example, if the energy of a primary photon is less than $\mathcal{E}_{\gamma min}$, the primary photon is more penetrating than the secondary photon. Thus in a test object whose dimension is about the same as the mean free path of a photon, the effect of multiple scattering is negligible.

It would be difficult to carry out a systematic treatment of the multiple scattering involving photoelectric effect, Compton scattering, and pair production. In spite of this complexity, an elaborate analysis of x-ray transmission in thick targets has been carried out analytically that shows how to correct the simple transmission rate Eq. (1), beyond its simplifying approximations. Fortunately, we now have an excellent Monte Carlo code (EGS4)

[22] developed at SLAC, which can be used to test its accuracy against the experimental data. Furthermore, this test helps us understand the detailed absorption and production mechanism of γ -rays for a given electron beam from the accelerator, such as PHERMEX facility at Los Alamos.

At high-energies $5\text{MeV} \geq \mathcal{E}_{\gamma m} \geq 1\text{MeV}$, where absorption by Compton scattering dominates, one may treat the multiple scattering as a series of small angle Compton scattering in which the photon energy loss is small for γ -rays that penetrate a large distance in the absorbing medium. With this approximation, the asymptotic solution for the transmission rate was obtained. It contains a factor $\exp^{-\mu_m x}$, a build-up factor, where μ_m is the smallest absorption coefficient for a given material (*e.g.*, μ_m is the absorption coefficient at 2.5 MeV for Pb). The build-up factor depends on whether the incident photon energy is greater or smaller than the energy at which the absorption coefficient is minimum [17, 23].

It is also well known that at very high energies ($\mathcal{E} \gg 10mc^2$), absorption by pair production dominates and thus the secondary Compton scattered photons may become more penetrating. Under this condition, the spectral equilibrium is controlled by the hardest secondary photons and the transmission takes a form $x^{-5/6} e^{-\mu_m x + bx^{1/2}}$, where $\mu_m = \mu(\lambda_m)$ is the minimum value at some wavelength (or energy) of an incident photon for any given material [26, 32, 33, 34]. Here the energy of an x-ray photon is related to its wavelength by $\mathcal{E}_{\gamma min} = hc/\lambda$, where h is Planck's constant. In laboratory units, $\lambda = 12.4 \times 10^{-3}/\mathcal{E}_{\gamma min}(\text{MeV})$, where λ is the wavelength in angstrom.

At extremely high energies, x-ray absorption by pair production becomes increasingly important. In this process, a photon creates an electron-positron pair which in turn can produce secondary photons by bremsstrahlung processes; the pair can also annihilate into two photons (*i.e.*, $e^- + e^+ \rightarrow 2\gamma$). The secondary photons can also undergo photo-absorption, Compton scattering or pair production, a phenomenon known as a photon cascade. The effects on the absorption coefficient of multiple scattering and photon cascades can be appreciable, depending on the range of an incident photon energy [13, 27, 35].

E. Reflection of X-Rays at a Sharp Boundary

In connection with Compton scattering of soft photons, we discuss the reflection of an x-ray beam at a sharp boundary by treating the x-ray beam as an incident electromagnetic

wave. A semi-classical analysis of the reflection of x-rays gives the index of refraction for x-rays as $n = 1 - \delta - i\beta$, where $\beta = \lambda\mu/(4\pi)$ and $\delta = 1/(4\pi)(e^2)/(mc^2)[(N_0\rho)/A][Z + \Delta f' \lambda^2]$. Here N_0 is the Avogadro's number, ρ the density, and A the atomic number weight, $\Delta f'$ is small away from the absorption edges [28]. Since the index of refraction is less than 1, the reflection can occur if the incident glancing angle is sufficiently small.

From Snell's law, the critical angle below which the total reflection can occur is determined by $\phi = \sqrt{2\delta} \simeq \rho_e^{1/2}\lambda$, where we have neglected the absorption term. This semi-classical analysis is often useful in identifying the reflection of soft x-rays from a bremsstrahlung source at a sharp boundary. For an x-ray wavelength of $1.03 \times 10^{-2}\text{\AA}$, the critical angle $\phi_{cr} \simeq 5.8 \times 10^{-5}\text{rad}$. As the incident glancing angle increases from the critical angle, the reflection intensity decreases.

F. Fluctuations of X-Ray Beam Intensity

An important refinement of the x-ray absorption process can be made from the observation that in a disordered medium the transmitted beam intensity shows a local fluctuation. Given the enormous amount of effort that has been devoted to the x-ray absorption mechanism, remarkably little is known about the nature of intensity fluctuations. The concept of localization of electrons in a solid was invoked in 1958 by Anderson to explain the electron transport phenomena in the presence of impurities [29]. The concept is usually associated with a disordered medium in which interference of multiple scattering of electrons by impurities give rise to enhanced backscattering.

We can see from Eq. (1) that apart from the K and L absorption edges the total cross section of the primary processes is a smooth function of an incident photon energy. The transmission rate Eq. (1) was derived based the single scattering approximation, which is valid as long as the mean free path of an incident photon for any given material is not small compared with the dimension of a test object. This implies that an independent, identical N atom model cannot explain the fluctuations of beam intensity. One final comment on the fluctuation of a transmitted x-ray intensity is note-worthy. Anderson localization was observed in experiments with a monochromatic light source [36, 37]. Unfortunately, the wide spectrum of a bremsstrahlung source can be a contributing factor to the intensity fluctuations but it is difficult to assess this effect. We can test our qualitative analysis of beam

transportation in a material in each step by using the code EGS4 [22] which incorporates many different absorption processes which are almost impossible to carry out a detailed analysis in practice.

IV. ABEL'S INTEGRAL EQUATION AND ITS SOLUTION

We now consider a symmetric cylinder whose material composition is uniform in the z -direction perpendicular to the incident x-ray beam and focus on an infinitely thin disk of the cylinder that is sufficiently far from the x-ray source. This allows one treat the x-ray source as a spatially uniform beam, which is an essential requirement for the derivation of Abel's integral equation [38]. Furthermore we assume that a detector accepts only those x-rays which traverse a narrow slice from the source (*i.e.*, a narrow beam approximation).

A. Abel's Integra Equation

For a pure absorption or a single scattering, the flux of an x-ray beam emerging from the disk, $I(y)$ along the slice is given by

$$I(y)\delta y\delta z = I_0\delta y\delta z \exp\left[-\int_{x_0}^{x_0} \mu(r)dx\right], \quad (2)$$

where I_0 is the flux of an incident monochromatic beam [see Figure 1] and is assumed to be independent of y , since we assume a uniform beam as an x-ray source. In Figure 2, $r^2 = x^2 + y^2$ and $x_0^2 = R^2 - y^2$, where R is the radius of the disk. We have also assumed the absorption coefficient $\mu(r)$ is cylindrically symmetric and hence our analysis is applicable to an one-dimensional problem, which is often misunderstood in practice.

Before displaying Abel's integral equation, which is the principal object of this paper, it is appropriate to comment on the narrow beam approximation. In an ideal situation, the transmitted x-ray intensity $I(y)$ must remain nearly monochromatic as the incident x-ray beam, since the scattered x-rays are assumed not to reach a detector (*i.e.*, a narrow beam approximation). In the presence of Compton scattering the narrow beam approximation breaks down if the scattering angle is large. This is the reason why we observe a diffuse background in an x-ray film.

If we define $f(y) = \ln(I_0/I)$, then Eq. (2) becomes

$$f(y) = 2 \int_0^{x_0} \mu(r) dx \quad (3)$$

Here $f(y)$ gives the sum of absorption or scattering along the slice. This quantity appears naturally in the integral equation for all observable which, like an x-ray absorption, represents strictly local interactions of x-rays with atoms. We shall therefore give a brief discussion of $f(y)$ itself, before returning to the details of Abel's integral equation.

In slab geometry, $f(y)$ remains positive or become zero if there is no absorption. In the presence of Compton scattering, $f(y)$ tends to give a value less than the expected value because of smear from the adjacent slices. Although the effect of Compton scattering is negligible in slab geometry (*i.e.*, a white noise), its effect becomes serious in a test object with a geometrical structure; $f(y)$ can give a negative value which signals a breakdown of a narrow beam approximation. Isolating $f(y)$ from the background in an x-ray transmission then requires the subtraction of the structure-dependent quantity, which is unknown *a priori*, a process requiring very accurate data analysis.

Let us now return to the derivation of the integral equation. If we eliminate the variable x in favor of r [see Figure 2], Eq. (3) can be written as

$$f(y) = 2 \int_y^R \frac{\mu(r)r dr}{(r^2 - y^2)^{1/2}}. \quad (4)$$

This is a form of Abel's integral equation [39].

B. Solutions to Abel's Integral Equation

With Abel's transformation, Volterra's solution to Eq. (4) is given as [1]

$$\mu(r) = -\frac{1}{\pi} \int_r^R \frac{f'(y)dy}{(y^2 - r^2)^{1/2}}, \quad (5)$$

where the prime on $f(y)$ denotes a differentiation with respect to its argument.

Equation (4) is our fundamental expression for the material absorption coefficient. Its equivalence to the x-ray emission from a hot plasma is clear from the derivation of Eq. (4) but can be made explicit by replacing $I(y) \leftrightarrow I_0(y)$ and $\mu(r) \leftrightarrow e(r)$ in Abel's integral equation. Thus Eq. (5) is applicable to both the radiation absorption and emission processes [1, 2, 3].

In practice, $f(y)$ is given as a set of discrete data taken from a detector or an x-ray film rather than as an analytic function. Normally, experimental data also contain a diffuse background (*i.e.*, random errors) due to Compton scattering or photon cascades. In the presence of fluctuations of a beam intensity, it is difficult to eliminate these errors either by Fourier-filtering or other numerical methods. The differentiation on the data points introduces spikes in noise in the integral. Thus a numerical representation of the data poses a difficult problem that must be treated with care. The numerical integration of Eq. (5) is best avoided entirely, if the numerical accuracy is desired.

Bockasten [4], and recently Wing [40] also recognized this point, but their calculations of polynomial fits of data points or expansion of the kernel of integral equation limit the accuracy of the results. As an alternative to the use of Eq. (5), Barr [8] obtained a solution of Eq. (4) by means of Abel's transformation. His solution allows one to devise an efficient smoothing method for data having a small random errors. His numerical algorithm eliminates the random errors after the integration, but before differentiation. This procedure ensures smooth results for a Gaussian type of density profiles. However, his solution is numerically unstable near the center. To overcome this difficulty we look for a different solution to Eq. (4) that is numerically more stable.

We start with the identity [39],

$$\frac{\pi}{\sin \mu\pi} = \int_0^\infty \frac{y^{\mu-1}}{1+y} dy, \quad (6)$$

where $0 < \mu < 1$.

By making a transformation $y = (z^2 - x^2)/(x^2 - \xi^2)$, we obtain

$$\frac{\pi}{\sin \mu\pi} = 2 \int_\xi^z \frac{x}{(z^2 - x^2)^{1-\mu}(x^2 - \xi^2)^\mu} dx. \quad (7)$$

For $\mu = 1/2$, Eq. (7) reduces to

$$\frac{\pi}{2} = \int_\xi^z \frac{x}{(z^2 - x^2)^{1/2}(x^2 - \xi^2)^{1/2}} dx. \quad (8)$$

Next we form a product integral

$$\begin{aligned} F(z) &= \int_z^R \frac{yf(y)dy}{(y^2 - z^2)^{1/2}} \\ &= 2 \int_z^R dy \int_y^R \frac{r\mu(r)ydr}{[(y^2 - z^2)(r^2 - y^2)]^{1/2}} \end{aligned} \quad (9a)$$

$$= \int_z^R r\mu(r)dr \left[\int_z^r \frac{ydy}{[(y^2 - z^2)(r^2 - y^2)]^{1/2}} \right] \quad (9b)$$

$$= \pi \int_z^R r\mu(r)dr, \quad (9c)$$

where we have used Dirichlet's formula [39] and Eq. (8).

Differentiating both sides of Eq. (9c), we obtain

$$z\mu(z) = -\frac{1}{\pi} \frac{\partial}{\partial z} \int_z^R \frac{yf(y)dy}{(y^2 - z^2)^{1/2}}, \quad (10)$$

which can be rewritten as

$$\mu(r) = -\frac{1}{\pi r} \frac{\partial}{\partial r} \int_r^R \frac{yf(y)dy}{(y^2 - r^2)^{1/2}}. \quad (11)$$

Here we notice that, in the limit $r \rightarrow 0$, $\mu(r)$ becomes numerically unstable, since $\mu(r)$ is indeterminate at the limit [8].

We now derive a different form of a solution to Abel's integral equation Eq. (4), which is equivalent to Eq. (5) but is less sensitive to random errors, and removes the difficulty in Barr's solution Eq. (11).

As before, we form a product integral

$$G(z) = \int_z^R \frac{z}{y} \frac{f(y)dy}{(y^2 - z^2)^{1/2}} \quad (12a)$$

$$= 2 \int_z^R dy \left[\frac{z}{y} \frac{1}{(y^2 - z^2)^{1/2}} \right] \int_y^R \frac{\mu(r)rdr}{(r^2 - y^2)^{1/2}}. \quad (12b)$$

By means of Dirichlet's formula [39], the integral can be rearranged as

$$G(z) = 2 \int_z^R dr\mu(r) \left[\int_z^r \frac{rzd y}{y[(r^2 - y^2)(y^2 - z^2)]^{1/2}} \right]. \quad (13)$$

With the transformation $[(r^2 - y^2)(y^2 - z^2)]^{1/2} = \eta(r^2 - y^2)$. the integral in the bracket [] can be evaluated by an elementary method, yielding

$$G(z) = \pi \int_z^R \mu(r)dr. \quad (14)$$

Thus we have

$$\int_z^R \frac{z}{y} \frac{f(y)dy}{(y^2 - z^2)^{1/2}} = \pi \int_z^R \mu(r)dr. \quad (15)$$

Using Eq (15) we derive the following equation by taking the advantage of the near continuous nature of the function $f(y)$ and with the similar transformation:

$$\mu(r) = -\frac{d}{dr} \mathcal{F}(r), \quad (16a)$$

$$\mathcal{F}(r) \equiv \frac{1}{\pi} \int_{r/R}^1 \frac{f(r/z)dz}{(1 - z^2)^{1/2}}. \quad (16b)$$

Some features of Eqs. (16) are similar to those of Barr, Eq. (11) [8]. While he starts with Abel's transformation, we start, however, from Dirichlet's formula [39] and carry out the final integral by an elementary method. An important point about this approach is that it avoids the direct differentiation of data points. Instead, we integrate over the data points, which, with proper choice of mesh points, smooths random errors in the data.

Next we show that Abel's integral equation admits three different forms of a solution, which are all equivalent as shown below:

$$F(r) - rG(r) = \int_z^R \frac{yf(y)dy}{(y^2 - r^2)^{1/2}} - \int_z^R \frac{r^2}{y} \frac{f(y)dy}{(y^2 - r^2)^{1/2}} \quad (17a)$$

$$= \int_r^R \frac{(y^2 - r^2)^{1/2}}{y} f(y)dy. \quad (17b)$$

Differentiating both sides of Eq. (17) with respect to r , we obtain

$$\frac{d}{dr} F(r) - G(r) - r \frac{d}{dr} G(r) = - \int_z^R \frac{r}{y} \frac{f(y)dy}{(y^2 - r^2)^{1/2}} \quad (18a)$$

$$= -G(r). \quad (18b)$$

Thus we have

$$\frac{d}{dr} G(r) = \frac{1}{r} \frac{d}{dr} F(r), \quad (19)$$

which shows that the solution by Barr [8] is equivalent to Eq. (15).

To show that Eq. (8) is equivalent to Volterra's solution, we integrate $F(r)$ by parts and obtain

$$F(r) = - \int_r^R (y^2 - r^2)^{1/2} f'(y)dy, \quad (20)$$

where the boundary condition $f(R) = 0$ was used.

Next we differentiate both sides of Eq. (20) and obtain

$$\frac{\partial}{\partial r} F(r) = r \int_r^R \frac{f'(y)}{(y^2 - r^2)^{1/2}} dy. \quad (21)$$

Hence we have

$$\frac{1}{\pi} \int_r^R \frac{f'(y)}{(y^2 - r^2)^{1/2}} dy = \frac{1}{\pi r} \frac{\partial}{\partial r} \int_r^R \frac{yf(y)}{(y^2 - r^2)^{1/2}} dy, \quad (22)$$

which completes the proof that there are indeed three different solutions to Eq. (4).

We may choose any one of the three solutions. The simplest numerical method, in principle, and the one that is least sensitive to small random errors, and the most computationally efficient method provide the criteria for selecting a particular form of the solution: Eq. (16) meets all of these criteria.

V. NUMERICAL METHODS

Before we proceed with the numerical computation, it is necessary to study the analytic structure of Eq. (4) and Eq. (16b). We see at once that both Eq. (4) and Eq. (16b) possess an end-point singularity. Therefore, the numerical accuracy will depend on how we treat the end-point singularities in these equations.

A. End-Point Singularity

We may proceed with our numerical calculations by either polynomial expansion of data points similar to Bockasten's method [4] or by carrying out the numerical integration for a given set of data by extrapolation (or interpolation). However, in the presence of fluctuations in the x-ray intensity, the former approach tends to introduce errors which are too large to neglect and leads to erroneous results. The latter approach suffers, of course, from the difficulty of treating the end-point singularity. Fortunately the numerical algorithm by Bickley [41] has been very useful for the evaluation of singular functions at the integral limits.

We carry out the numerical integrations of Eq. (4) and Eq. (16b) using the numerical scheme of Jeffereys and Jeffereys [41], which employ Bickley's formula near the integral limits and carry out the remaining integral by the Gregory formula. A more elaborate but

similar end-point formula has been also developed by Young [42]. However, we prefer that of Jeffereys and Jeffereys [41], because it is easier to adapt to different sets of experimental data.

Next we discuss the steps to reduce the raw experimental data to properly extracted data for numerical analysis. There are two aspects in the processing experimental data: a selection of necessary data points and optimum background removal. The selection of data points to carry out the numerical integration and differentiation depends on the numerical algorithm. In most experiments, data taken from an x-ray film provide a sufficient number of data points. By three point interpolation or extrapolation, we set the data at the cell boundaries for the integrations and carry out the differentiation at the cell centers. This process effectively smoothes the data in the short wavelength regime, but it preserves the fluctuation in the long wavelength regime. In particular, this numerical scheme is useful for any type of background removal (*e.g.*, white noise), and to make certain that there are no oscillations in the background whose frequencies are much higher than those of fluctuations in the data.

B. Numerical Tests of Self-Consistency

Eq. (4) and Eq. (16b) play critical roles in the present work. To check the self-consistency of the numerical code, we have calculated $f(y)$ based on a theoretically model given by Eq. (4), which are in turn, used to calculate the absorption coefficients from Eq. (16b).

In the absence of appreciable noise in $f(y)$, the code calculates the precise profiles of the absorption coefficients (see Figures 5 and 6; and Figures 9 and 10). It should be noticed that Eq. (4) has the same analytic structure as Eq. (16b), and that the same subroutine in the code can be used to compute both $f(y)$ and $\mathcal{F}(r)$.

The advantage of using the theoretical values $f(y)$ (*i.e.*, instead of a true experimental value in slab geometry) is that they can be calculated without including effects of wide spectrum of an x-ray source and Compton scattering of photons with electrons in a metal. Moreover they can be used to see if a significant amount of noise is present in the experimental data. Thus this intermediate step of analyzing the experimental data is extremely useful for identifying the large angle Compton scattering effects.

VI. NUMERICAL CALCULATIONS OF ABSORPTION COEFFICIENTS

A. Experimental Data

Within the limits of our approximation on the x-ray absorption mechanism (*i.e.*, neglecting the effects of multiple scattering and photon cascades since these effects are extremely small in the present experiment), we may calculate the absorption coefficients from the experimental data. However there are several other important effects which we must address: first we have assumed the x-ray source is monochromatic in the derivation Eq. (1) to calculate $f(y)$. This is perhaps the most serious assumption of the approximations made in the derivation of Abel's integral equation. This assumption together with the spatial uniformity of the x-ray beam is essential for the determination of absorption coefficients for any given material by means of Abel's inversion, since the absorption coefficients for any given material depend on the photon energy of x-ray source. The spatial uniformity requires a point source of an x-ray which is the major challenge for an accelerator physicist because the point source requires a pencil beam of a high energy electron in a high current accelerator (*e.g.*, PHERMEX at Los Alamos) [44]. Hence the basic assumption of a monochromatic x-ray source is hard to achieve, since the bremsstrahlung source has a wide spectrum; the x-ray spectrum spans the entire energy range from an incident electron beam energy of an accelerator to zero (*e.g.*, 30 MeV to zero in PHERMEX). In other words, the bremsstrahlung spectrum is fairly flat function of photon energy.

1. Progressive Filtering

If the x-ray intensity at a great depth from a bremsstrahlung source depends on multiple scattering, the beam intensity tends to reach an equilibrium state (*i.e.*, the progressive formation and decay of the hardest secondary soft photons). The reason for this process is that the progressive filtering of an x-ray beam from a bremsstrahlung source tends to make the attenuation curve steeper than $e^{-\mu x}$, but the secondary photons from Compton scattering can compensate for the steepening if the beam penetrates to a great depth to allow the multiple scattering. For example, the mean free path of the average photon energy of 1.2 MeV in U^{238} is approximately 1.14cm, which is roughly equal to the size of test object, the effect of the progressive filtering of an x-ray beam by the test object cannot be

compensated for by any simple physical mechanism.

2. *Effects of a Void*

Next we turn to a discussion of an x-ray transmission in a material with a void whose radius is much larger than the coherence length of a disordered medium. The effect of the void on the absorption coefficients is similar to the surface absorption in that incident x-rays see a concave surface where a partial reflection of the x-rays can occur [28] and the primary photons may lose its energy by Compton scattering at a large scattering angle near the surface (*i.e.*, a reflection of x-rays at the sharp boundary). It differs, however, in that the net effect of progressive filtering and Compton scattering of photon depends on a geometrical structure factor. The presence of a sharp boundary leads to multiple reflections of soft photons in a void such that an assumed free propagation of photons without a reflection is no longer appropriate, *i.e.*, a radiation trap.

Hence the spatial analysis given in Cormack's paper [9] requires a proper correction at the interface between aluminum and Lucite because of a sharp boundary between them. In addition, the calculation is invalid because of the ill-defined gamma ray source which should be assumed to be spatially uniform to make use of Abel's inversion. Although the spectrum of Co^{60} source is not as wide as bremsstrahlung source, the gamma ray beam still experience a partial reflection at a sharp boundary.

3. *Experimental Determination of the undesirable Effects*

The present work was undertaken to study the above undesirable effects experimentally. In particular, to investigate a possible beam intensity fluctuations, we have selected metallic U^{238} cylinder, which contains a small fraction of impurities that simulate a random, disordered medium. The schematic picture of the experimental arrangement is given in Figure 1. The test object is a cylinder of U^{238} , 2 *in* long and 0.5 *in* diameter with holes on both ends is exposed to a high energy x-ray source with the average energy of photons $\mathcal{E}_\gamma \simeq 1.2MeV$. The x-ray beam emerging from the test object enters a photographic plate through 0.25 *in* thick lead filter, 3 m down stream from the x-ray source. The data from the x-ray film were then taken, with a microdensitometer digitized, and then processed by a minicomputer to

eliminate the background. Experimental data sets for both solid and hollow disks are given in Figures 3 and 4, to which a digital noise reduction technique has not been applied.

B. Theoretical Values Vs Experimental Data

In Figures 5 and 6, we show $f(y)$ as a function of y by Eq. (4) with $\mu = 0.875/cm$ for a cylinder of U^{238} . In order to see the details of discrepancy between the experimental data and the theoretical values, we have also computed $f_{exp}(y)$ from the experimental data, which is displayed in Figures 7 and 8.

The quality of $f_{exp}(y)$ should be critically examined by comparing it with $f(y)$. First we see from Figures 5 and 7 that $f_{exp}(y)$ shows a long tail extending beyond the outer boundary.

Crucial to any x-ray diagnostics is the calibration of the measured transmitted beam and source intensities. This can be done either with the theory using a measured absorption coefficient from a slab geometry or empirically from the measured standards. The reason for this is the difficulty of estimating the incident flux intensity I_0 which varies from shot to shot in a Bremsstrahlung source. The basic goal in determining I_0 is to match as closely as possible the ideal situation of measurements in the slab geometry.

The long tail in Figure 7 clearly suggests that the calibration for $f_{exp}(y)$ was seriously in error, because $f_{exp}(y)$ must be zero at the outer surface and become negative beyond the boundary due to Compton scattering at the surface.

Next we observe that f_{exp} exhibits the intensity fluctuation which, we believe, is due to enhanced backscattering in a disordered medium (Anderson localization [29]). In the experimental data on Carbon reported by several different groups [43], one notices a wide range of disagreement in the absorption coefficients. In an experiment with Carbon, one must be concerned with x-ray absorption in a disordered medium (*i.e.*, due to a random distribution of small voids). We believe the disagreement can be attributed to Anderson localization, which implies a breakdown of a model of N independent, identical atoms for a medium. This is a macroscopic realization of quantum many-body effects in a disordered medium.

Furthermore, the recent experiments of light propagation in a disordered medium [36, 37] provide direct evidence of enhanced backscattering with the light intensity fluctuation which are very sensitive to the pattern of speckles in the medium. These measurements are

consistent with our data, which suggests that the x-ray intensity fluctuations are due mostly to impurities in U^{238} and partly by the broad spectrum of the bremsstrahlung source.

If we compare Figures 5 and 7, we can clearly see the effects of progressive filtering and large angle Compton scattering; the breakdown of the narrow beam approximation is particularly evident. An important question concerning the use of x-ray radiography for quantitative determination of a density profile is how accurately both the progressive filtering and Compton scattering effects can be determined and their contribution eliminated. If they can be accurately accounted for, then, only then, the remaining data can provide a density profile within the limit of the narrow beam approximation.

We observe from Figures 5 and 7 that the breakdown of the transmission rate, Eq. (1), increases as r approaches the center of a test object. We also see appreciable effects of Compton scattering at the edge, which produce a diffuse boundary. This shows that one cannot hope to isolate these effects by a simple numerical method or background removal, and thereby obtain precise absorption coefficients by Abel's inversion. These effects must be corrected by filtering technique that can keep the spectrum width $\Delta\lambda$ as small as possible; this eliminates the progressive filtering by a test object.

By placing an appropriate filter in front of a film, we may further reduce the effect of Compton scattering at the edge. Again, what has been said about the Compton scattering effect also applies to the curved surface of a test object in which an oblique incidence of an x-ray beam leads to a partial reflection of the beam. This can be corrected only by an analytic method.

Comparing Figures 6 and 8 we observe similar effects in $f_{exp}(y)$ for a hollow cylinder, but a large discrepancy between $f_{exp}(y)$ and $f(y)$ exists near the center extending to the boundary of the void. In the absence of dense material at the center of the test object, the peculiarly strong absorption of x-rays at the void can be explained only in terms of the multiple reflection of soft x-rays at the sharp boundary (i.e., a radiation trap), as will be discussed later.

The absorption coefficient μ in the numerical calculation of $f(y)$ was measured in the slab geometry in which the surface scattering effects are subtracted by adjusting $I_{true} = I_0 - \delta I_0$ where δI_0 is a correction term. Although considerable accuracy of the experimental values has been achieved from such measurements, similar measurements using an object with a geometrical structure do not provide the same degree of accuracy, partly because we are not

able to find a reasonably accurate analytical form for δI_0 .

Contrary to common belief, the significant discrepancy between $f_{exp}(y)$ and $f(y)$ in the presence of a void in materials does not involve spatial resolution in connection with the spot size of an x-ray source, but is instead due to both Compton scattering and the progressive filtering. This is evident because we can still locate the boundaries of a test object whose dimension is less than the spot size.

Finally we have calculated the absorption coefficients for both a solid cylinder Figure 9 and a cylinder with a void at the center Figure 10 using the numerical code developed based on the Eqs. (16). The results clearly show that Eqs. (16) are indeed a correct solution to the Abel's integral equation Eq. (4) and the numerical accuracy of the code is indeed impressive.

C. Computation of Absorption Coefficients from Experimental Data

By means of Abel's inversion Eqs. (16), the absorption coefficients are computed from the experimental data with the code and are shown in Figures 11 and 12. Analyzing the data from the computed absorption coefficients has the advantage by comparing with Figures 9 and 10 in that one clearly sees the effects of enhanced backscattering and Compton scattering.

The main result obtained from this numerical computation of the absorption coefficients is the demonstration of a strikingly accurate numerical algorithm that treats the random noise without any sign of amplification. Moreover, the calculated absorption coefficients show a consistency with the experimental data.

Figure 11 shows the calculated absorption coefficient as a function of radius for the solid cylinder of U^{238} . Several important qualitative conclusions can be drawn from the figure. First of all, the variation of the calculated absorption coefficient exhibits irregular patterns containing a smooth oscillation in each isolated region, a phenomenon that can only arise as a result of enhanced backscattering in a disordered medium. Moreover, the calculated absorption coefficient reflects a small but pronounced local fluctuation in the x-ray intensity in the medium.

As mentioned earlier, such an effect has also been observed in the experiments on the multiple scattering of visible light by an aqueous suspension of sub-micrometer size monodisperse polystyrene spheres [36, 37]. These experiments confirmed the enhanced backscat-

tering of light waves by disordered scattering centers in a medium.

A qualitative picture of the dependence of the correction term δI_0 on the glancing angle can be inferred, for the energy region of our interest, from the surface reflection phenomenon at x-ray energies less than 10 keV [28]. The shape of δI_0 sensitively depends on the incident photon energy and glancing angles less than the critical angle (above which there is no reflection). By adjusting the correction term to give the theoretical values $f(y)$ in closer agreement with the experimental data, one learns which physical processes are responsible for the various peculiarities in the data.

For the same cylinder with a void, the absorption coefficient calculated from the experimental data is shown in Figure 12. The effect of a partial reflection of x-rays at the boundary of a void can be clearly seen. The error in the absorption coefficient is about 52 % at the center, which appears to suggest the presence of radiation absorbing material. This significant disagreement between the computed value and the expected value (Figure 12) reflects the neglect, in this simple form of absorption mechanism, of the fundamental physics treating a void in a medium or suggests an error in the calibration of the measured transmitted beam and source intensities, or both. As explained above, the calibration of the experimental data is clearly in serious error. A proper calibration would have reduced the error in the absorption coefficient to less than 30 %.

Any simple physical process that may have been involved in this x-ray transmission is not abstruse, since one notices that the reflection of an incident x-ray beam at the outer and inner surfaces can reduce the transmitted beam intensity significantly. The maximum reflection takes place at the edge of a void where the glancing angle becomes nearly equal to the critical glancing angle [28]. As the glancing angle increases, the effect of x-ray reflections reduces. It should be emphasized that a bremsstrahlung source is far from being monochromatic as we will discuss later. Thus soft x-rays, whose critical glancing angles are much larger than those of hard x-rays, will reflect more readily at the surfaces. For high-energy photons, the angular dependence of scattered photons must be analyzed by the Klein-Nishina formula [16].

It is straightforward to assess the effect of Compton scattering at a sharp boundary for a monochromatic source, but it becomes prohibitively difficult for a bremsstrahlung source. Thus we can see that Compton scattering at a sharp boundary leads the breakdown of the basic assumptions of x-ray transmission in the void for which EGS4 can be utilized to see

the effect of the bremsstrahlung source. In passing we note that, in Compton scattering experiment, a target of circular cross section such as cylinder is often used for the study of angular dependence; the scattering center at the surface is better defined even if the beam is poorly collimated. However, as we have seen in our data analysis, accurate evaluation of the flux intensity at the target is difficult.

We are thus faced with a question: how does the x-ray reflection at the surface of a void differ from that of the outer surface? Moreover, in the presence of photo-emitted electrons, how are we to describe the x-ray transmission in the void? To answer these questions we must focus on the nature of interactions of photons at the surface and in the free space of the void.

The incident x-rays see the concave surface, where a partial reflection of the primary and secondary photons can take place. A fraction of the primary and secondary photons are ultimately absorbed near the boundary of a void, giving rise to enhanced photoemission of electrons in the void. We also note that, in the absence of a strong Coulomb field of nucleus, no pair-production can occur in the void.

Furthermore, Compton scattering of primary and reflected photons by photo-emitted electrons in the void is small compared with that of condensed matter, but it can be a contributing factor to the discrepancy, since the trapped photon intensity is much larger than the primary x-ray beam intensity for a small void.

In general, as expected, the effect of the x-ray reflections on the transmitted beam intensity is less severe as the radius of a void increases. This can be easily understood by the fact that the x-ray reflection takes place near the edge. An important point to notice is that near the edge of the void we see a significant dip in the absorption coefficient which shows the reflection of x-rays. In summary, *we have shown that a numerical calculation of density profile by Abel's inversion has its limitation and cannot be used as a quantitative tool for a hydrodynamic test!* The conventional approach to examine the film by experienced eyes will provide a better diagnosis for a hydrodynamic test. The noise is inherently too large in its magnitude to neglect. In addition, a three-dimensional density profile of a test object cannot be obtained in an environment of a dynamical test of hydrodynamics as discussed below.

VII. OPTIMAL EXPERIMENTAL CONDITIONS

In order to obtain reasonably accurate absorption coefficients from the experimental data by means of Abel's inversion, the most optimal experimental condition must be realized so that the data to be analyzed are free of significant distortion.

To derive the Abel's integral equation Eq. (4), several simplifying assumptions are made. We examine the assumptions to minimize the errors that they introduce and to find the optimal experimental conditions.

The most serious approximation made was to assume that a bremsstrahlung source is monochromatic. The potential difficulty introduced by this assumption can be appreciated if we recall that a bremsstrahlung source spans the entire spectrum exhibiting a relatively flat intensity profile with respect to photon energy [14]. Furthermore an absorption coefficient for any given material depends on photon energy and Z -number. Thus it is important to limit the width of the spectrum to the smallest possible value.

There are several technique for limiting the wavelength range $\delta\lambda$ available, with each its advantages and disadvantages. The simplest method is to use a crystal monochromater. However this would be impractical in our x-ray diagnostics, because the wavelength of our x-rays is too short compared with a lattice parameter of available material.

From Fig. 32 of Bethe and Ashkin [17] we see that there is a region of maximum transparency for all material (MTM) which lies between 2.5 MeV and 10 MeV. This is admittedly a rather loosely defined spectral range, its limit being in principle different for each metal, but one may think of the spectral range as the window of maximum transparency for heavy materials. In the language of scattering theory, one can say that while at high energies (*i.e.*, $\mathcal{E}_\gamma \gg 10MeV$) the mean free path is so small that for a thick target a photon must undergo multiple scattering to reach a detector. As the photon energy is lowered into the region of MTM the photon mean path is sufficiently large that the effect of multiple scattering can be negligible. As discussed earlier, the transmission rate defined in Eq. (1) does not admit multiple scattering, which can be a serious effect for a thick targets. Because the x-rays in the region of MTM can penetrate to a great depth without significant multiple scattering, a varying photon energy $\langle\mathcal{E}\rangle_{av}$ can cover many blemishes in Abel's integral equation. Thus the solution of the integral equation can give a reasonably reliable absorption coefficient apart from the large angle Compton scattering which can be eliminated without difficulty.

This discussion has an important implication with respect to a design of an x-ray source for an x-ray diagnostics. The basic goal in selecting $\langle \mathcal{E} \rangle_{av}$ is to match as closely as possible the upper limit of the region of MTM with the smallest possible spectral width. Since the maximum photon energy in a bremsstrahlung source is nearly equal to an incident electron beam energy hitting a tungsten target, the upper limit can be set by selecting a specific electron energy.

A better technique than a monochromater for reducing the spectral width is to use filtering materials by which the photons with energy less than 5 MeV are eliminated and Compton effects are minimized. It is important to note that since the same absorption coefficient can be measured at two different energies in this region, we must block the low energy photons before they reach a test object. This is possible because the x-rays to be filtered are of higher energy than the fluorescent signal.

By choosing an appropriate filter, its absorption edge can be placed between the photon energy (to be filtered) and fluorescent energies, preferentially absorbing the former. The major difficulty with this method of x-ray filtering is that absorbed x-rays can be re-emitted as fluorescent radiation that is relatively un-attenuated by filters and strike film to increase the fog level. This degrades the sensitivity to low level signals. It should be emphasized, however, that by eliminating the soft photons we reduce both progressive filtering and Compton effects at the surface of a test object and that the filtering improves the quality of data considerably.

On the other hand, the filtering reduces the source brightness, which is defined as the number of photons emitted per unit solid angle. Empirically it is found that the bremsstrahlung radiation intensity in terms of the electron beam energy in the forward direction is given $I_\gamma \propto I_e \mathcal{E}_{kin}^{2.9}$, where I_e is the electron beam intensity and \mathcal{E}_{kin} is the electron kinetic energy in unit of mc^2 [14]. Here the target material was gold. We can appreciate from the above empirical formula and Fig. 30 of Koch and Motz [14] that, for example, at a given electron beam energy it is necessary to increase the current intensity in order to maintain the same effective source brightness.

This requirement poses a difficult problem for which the accelerator community is in search of an answer - a new acceleration mechanism capable of generating an intense relativistic beam. Fortunately, a novel acceleration developed by Friedman [45, 46] has been tested in experiments demonstrating that a beam of electron current of 70 kA can be ac-

celerated to a energy of 7 MeV. However, it was found that the acceleration mechanism is not scalable to higher energy due to various instabilities.

The unique feature of the auto-acceleration mechanism is that the electromagnetic field for the acceleration is created by the interaction of the first electron beam with a cavity. The electromagnetic field energy is then transferred to the second electron beam in the same structure, producing a short pulsed (*e.g.*, 20 ns), intense electron beam. Moreover, the auto-accelerator circumvents the two major problems in pulsed power accelerators - the fast switches and insulators; the accelerator is automatically self-synchronized and thus eliminates the jitter due to the switches.

It should be stressed, however, that the efficiency of the auto-acceleration mechanism depends on the ratio of the first beam intensity to that of the second. Since the extracted electromagnetic field energy from the first beam is the only source of the acceleration for the second beam, the larger the ratio, therefore, the more efficient the auto-acceleration is bound to become.

Consideration of the stability of an intense relativistic electron beam in a structure led Friedman [46] to the modification of previous experiments. In a recent experiment [46], the first beam was modulated by using an external rf source to enhance the interaction between the beam and the modified structure. Hence the accelerated beam and the modulated beam exchange energy through the modified structure while moving on different trajectories. Friedman has demonstrated that the accelerated beam of 200 Å attains the kinetic energy of 60 MeV with the beam radius of 0.1 cm. This result strongly suggest that there exists a domain of parameters in which we can select an appropriate accelerated beam intensity for an optimally useful x-ray source.

We now examine in some detail the characteristics of of an intense electron beam for an x-ray source for the radiography: first, we study the efficiency of bremsstrahlung production for a given beam energy, which is defined as the ratio of the total bremsstrahlung radiation emitted to the total energy of an incident electron beam and is given by $\epsilon = 3.0 \times 10^{-4} Z \mathcal{E}_0 / (1.0 + 3.0 \times 10^{-4} Z \mathcal{E}_0)$ where \mathcal{E}_0 is the kinetic energy of an incident electron [14]. The efficiency depends on the target material and the kinetic energy of an incident electron beam. For example, the efficiency $\epsilon = 31\%$ at $\mathcal{E}_0 = 20mc^2$ but it is 41% at $\mathcal{E}_0 = 30mc^2$ for Pt targets. Note also that the spectrum shape of bremsstrahlung intensity is given by $S = 1 - \exp -\mathcal{E}_0 / [51(\mathcal{E}_0 - \epsilon_0)\epsilon_0^2]$, where $\mathcal{E}_0 - \epsilon_0 = h\nu$, ν is the frequency of a

photon emitted in the forward direction, and h is Plank's constant [14].

Thus for 10 MeV electron beam incident on a thick tungsten target, the efficiency $\epsilon = 30\%$ and about 35% of photons emitted in the bremsstrahlung process have their energy higher than 5 MeV. In the x-ray transmission, unfiltered soft photons are absorbed through progressive filtering in a test object and do not reach a detector. Assuming the spectrum width $\delta\lambda = 1.24 \times 10^2 \text{Å}$, which is equivalent to 1 MeV, the optimally useful x-rays are, therefore, 15% to 25% of the total photons emitted in the bremsstrahlung processes.

At extremely high electron beam energies like the one in the PHERMEX facility (the electron beam current $\mathcal{I}_e = 2.8 \text{kA}$ and the electron energy ($\mathcal{E}_0 = 30 \text{MeV}$), the radiation cone from a bremsstrahlung source is extremely narrow and x-ray photons are emitted mostly in the forward direction. Thus spectrum shape can be described by the above analytic expression which shows the peak intensity in the energy range of 5 MeV to 6 MeV. It should be remarked, however, that although the efficiency for this beam is $\epsilon = 57\%$, hard γ -rays from a bremsstrahlung process tend to cascade in a test object and the x-ray transmission is controlled mainly by the photons with energy in the neighborhood of the peak intensity and hardest secondary photons are produced in multiple scattering. These examples are given to show certain features that provide a qualitative picture to identify an optimally useful x-ray source. Again, one may try to use EGS4 code to check if the above qualitative picture holds for a target design of a bremsstrahlung source.

The above analysis shows that the high-current, high-energy electron beam is obviously preferred for an optimally useful x-ray source and the only remaining question that concerns if the photon energy falls in the region of MTM.

The second issue is the more fundamental problem, which is common in all high-current accelerators; it is important to focus an electron beam to obtain uniformly, diverging x-ray beam to satisfy the assumption of a parallel x-ray beam. Although it is extremely difficult, one should be able to achieve a small spot size by the combined use of a quadrupole magnet and ion focusing [10, 47].

We also note that the shape of radiation cone from bremsstrahlung processes depends on the incident electron beam energy and that, with an electron beam energy in the region of MTM, the radiation cone is sufficiently large that the x-ray beam diverges uniformly in space. This is a critical factor for the spatial uniformity of the x-ray beam, which is the basic assumption in deriving Abel's integral equation.

In the light of the above problem, it is essential to develop a simple, reliable acceleration mechanism such as Friedman's auto-acceleration mechanism. Indeed, the simplicity and the efficiency of the auto-acceleration mechanism hold out the hope that one might develop an x-ray source that meets the requirements. Clearly the auto-acceleration mechanism shows definite advantages over a more conventional rf linac for generating a high-current, high-energy electron beam. Moreover, this type of accelerator is compact and inexpensive to build compared to an rf linac.

We would like to emphasize, at the end of this detailed discussion on the optimal condition for an x-ray source, that the physics and experimental technique elaborated here provide a starting point from which we can develop an optimally useful x-ray source with narrow spectrum width and adequate beam intensity.

VIII. DISCUSSION AND CONCLUSION

Although our analysis of the experimental data is qualitative in nature, we have attempted to quantify the discrepancy from the form of transmission rate $I = I_0 e^{-\mu x}$, by using Abel's inversion Eqs. (16) and its numerical solution. Given the large uncertainties due to the lack of detailed understanding of the physical processes in the x-ray transmission for a given test object with a structure as well as the limited data, our interpretation should be taken as only suggestive.

One of the major problems that confronted us in this experiment was the complexity of the acquisition and interpretation of the experimental data. Abel's inversion is conceptually simple and mathematically straightforward. Qualitative though this picture may be, as it has to be, since a simplified transmission of γ -rays in material cannot hold true even in its first-order analysis. The lack of detailed agreement between the theory based on the a simple x-ray transmission rate and the experimental data, however, shows a complexity of transmission of radiation in high Z-material. Since the x-ray transmission itself is inherently complex a phenomenon, there seems little hope to achieve the reliability required for a quantitative method in x-ray diagnostics in hydrodynamics. *Thus it is highly unlikely that the quantitative diagnostic by the radiographic method in hydrodynamic test can be meaningful.* In practice, it can be misleading.

That the experimental measurements are not always reliable themselves is not an im-

portant issue, since the most optimal condition can be realized, and perhaps reliable data can be obtained. Even under the best condition, the data cannot still satisfy the basic assumption on Abel's inversion. In general, several different corrections must be made to the directly observed transmitted x-ray intensity in order to obtain a reasonably credible absorption coefficient by Abel's inversion.

It should be emphasized, however, that, in most experiments, I_0 and $I(x)$ are read simultaneously from a film, and that the incident and the transmitted x-ray beam intensities are assumed to be nearly monochromatic, which is far from being true. This requirement of an x-ray source is essential for the measurement of absorption coefficients, which depend on the average energy of an incident photons. Numerous simplifying approximations (*e.g.*, the narrow beam approximation, *etc.*) have been made for reasons of both availability of an x-ray source and expediency. There is no practical method to produce monochromatic x-ray beam. The final effects of these approximations remain unknown.

Application of Abel's inversion in x-ray diagnostics is not as straightforward as for plasma diagnostics since we do not know how to make corrections to the transmitted x-ray intensity. Sometimes one might get the impression that the correction to the transmitted beam intensity, δI , is something of an art. For the worst case this is probably true.

One must therefore exercise the scientific prudence by checking every step with the Monte Carlo code EGS4 [22] to insure that the corrections are well justified and are in the order of procedures weighted by the importance of the processes: a) an incident x-ray beam intensity; b) removal of background due to photon cascade; c) Compton scattering at a sharp boundary; d) progressive filtering due to a finite spectrum width; e) a narrow beam approximation.

The relative importance of each of these corrections, as well as the details of correction procedure, depends on the x-ray beam energy and the particular material composition of a test object. Unfortunately, little discussion of these corrections has been attempted in most of the published measurements of x-ray transmission. This has greatly impeded progress in x-ray diagnostics.

A crucial question concerning the application of Abel's inversion for quantitative x-ray radiography is how accurately the Compton effects such as partial reflection of x-rays at a sharp boundary and x-ray scattering at the edge can be determined and can be corrected. Unfortunately the most difficult quantity to measure in x-ray radiography is an accurate

incident x-ray beam intensity I_0 . A variety of effects can distort the incident beam intensity profile severely while leaving the energy spectrum relatively undisturbed. Yet it is the incident beam intensity that is critical factor in determining the absorption coefficients by Abel's inversion.

As explained earlier, the reflected x-ray beam intensity at a sharp boundary varies with the incident glancing angles larger than the critical angle ϕ_{crt} . This implies that δI with a test object having a curved surface depends on the geometrical structure factor which is extremely difficult to determine.

Any background removal method has the potential of distorting the data. It is therefore important to isolate each contribution to the correction term by combined use of analytic method and EGS4 code. For example, some of the strongest Compton scattering effects occur at the outer edge, where they are caused by the total reflection of an x-ray beam. Occasionally the simplest remedy for this Compton effect is, albeit difficult in some instances, to place an appropriate filter in front of a film. One can see the effect with the clarity of an improved image.

On the other hand, with the data having contributions from progressive filtering of photons, it may be difficult to find a simple remedy that can isolate the filtering effects. One notices from the absorption curves of metals (see Fig. 32 of Ref. [17]) that one should not use an average photon energy for the calculation of absorption coefficients unless the spectrum width of an x-ray source is small. One should have expected that, in addition to the progressive filtering, the narrow beam approximation [Eq. (1)] will break down in this most unfavorable case, *i.e.*, a bremsstrahlung source without filtering.

The difference between the absorption coefficients calculated from experimental data taken for a cylindrical test object and the experimental value determined in slab geometry is quite significant, suggesting that the major effect (*e.g.*, Compton scattering by free and bound electrons at large scattering angles) in the presence of a sharp boundary was not taken into account.

Because of this, it is essential to find the method that is consistent and systematic in the selection of parameters for δI . This can be achieved by analytic study of the reflection and absorption of x-rays at the surface of a test object and systematic experimental tests for various test objects. It is imperative, albeit tedious, to make several attempts at background removal with different sets of parameters, follow each set of experimental data through the

entire analysis for different test objects, and test the results for consistency.

Although the calculation of $f_{ex}(y)$ is an intermediate step in Abel's inversion, a great deal of information may be gained by direct inspection. For test objects with small amount of impurities, the theoretical value $f(y)$ calculated from Eq. (3) using the experimental value μ determined in slab geometry can be used for a comparison with $f_{ex}(y)$. This comparison will show the fluctuations in the transmitted x-ray intensity and diffuse boundaries. This exercise is useful as an overview of the data, yielding the information about a possible form of correction to the incident x-ray intensity. Inspection of $f_{ex}(y)$ is also useful as a check of the x-ray beam profile.

The fluctuations in x-ray beam intensity, which should not be confused with statistical fluctuation of noise [48], are intrinsic phenomena which one should not apply a smoothing technique in any data analysis; the fluctuations reflect the property of a material, for example Anderson's localization by impurities.

Next, it should be stressed that Abel's integral equation derived from the simple x-ray transmission rate Eq. (1) does not admit multiple scattering which can modify the transmission equation significantly. As a general guide in the design of experimental x-ray transmission measurements, we may find it useful to check if the dimension of a test object is less than $5\lambda_{mfp}$, the mean free path of a photon at a given energy. For a thin target, the multiple scattering can be safely neglected. One may not be able to neglect the multiple scattering, however, in a thick target (*e.g.*, a size larger than $10\lambda_{mfp}$). The error introduced in Eq. (1) by the multiple scattering will enter into the later calculation of the absorption coefficients of materials by Abel's inversion. Such a check can be easily made by referring to a published x-ray absorption coefficient table for metals and a systematic test with EGS4 code.

Finally, we have shown how we may obtain one-dimensional density profile by computing the absorption coefficient with Abel's inversion Eq. (16) from two-dimensional x-ray film for a cylindrically symmetric object in one x-ray exposure for which an x-ray source is located in a sufficiently far distance from a test object to insure a parallel beam. There is little need to see a two-dimensional density profile in a radiography, since we can easily obtain the two-dimensional view in one x-ray exposure. A question naturally arises, however, how one may obtain a three-dimensional density profile that is quite useful in non-invasive diagnosis such as in medicine. Since the wave number $k_\theta = m/r$ in cylindrical coordinates,

the spatial resolution requires that *the m exposure by rotating the x-ray source about the axis (z -direction) to obtain the three-dimensional density profile.* This requirement was misunderstood in his study of a line integral for application of to radiological application by Cormack [9] and thus his analysis is invalid. The m different views provide the necessary information on density profile in each direction which can be used to construct the three-dimensional density profile as in a three-dimensional radiographic machine. For a given mode number, the best spatial resolution will be achieved near the axis of symmetry. A rule of thumb on the spatial resolutions is: the larger the number of exposures m is, the more reliable the three-dimensional density profile will be in a numerical reconstruction [49]. This can be achieved either by rotating an x-ray source or rotating a test object, which is not feasible in any dynamic hydrodynamic test. This analysis does clear up the myth that one may be able to build a 3-D hydrodynamic test facility with the two x-ray sources which is known as the Dual Axis Radiographic Hydrodynamic Test Facility or DARHT project at Los Alamos [38].

-
- [1] H. Hörman, Z Physik **97**, 539 (1935) and V. Volterra, *Lecons sur les Equations Integrale et les Equations integro-differentielles (Paris, 1913)* p34
 - [2] H. Maecker, Z. Physik **136**, 119 (1953); **139**, 448 (1954).
 - [3] J. Friedlich, Ann. Phys. **3**, 327 (1959).
 - [4] K. Bockasten, J. Opt. Soc. of Am. **51**, 943 (1961).
 - [5] R. N. Bracewell, Aust. J. Physics **9**, 198 (1956).
 - [6] J. Chang, *et al.*, Appl. Phys. Lett. **39**, 279 (1981).
 - [7] N. C. Luhman and W. A. Peebles, Rev. Sci. Instr. **55**, 279 (1984); Chul Park and D. Moore, NASA TN DW-5677 (1970).
 - [8] W. L. Barr, J. Opt. Soc. of Am. **52**, 885 (1962).
 - [9] A. M. Cormack, J. Applied Physics, **34**, 2722 (1963); **35**, 2908 (1964).
 - [10] S. J. Han (LA-UR-93-2146); Steven Weinberg, J. Math. Phys. **8**, 614 (1967).
 - [11] One should be aware of the assumption of a paralell incident x-ray beam which is produced at a far distant by a point source. Hence one cannot apply a Fourier decomposition on the angular dependence in Cormack's Equation 2.

- [12] D. C. Koningsberger and R. Prins, *X-ray absorption: Principles, Applications, Technique of EXAFS, SEXAFS, and XANES* (John Wiley, New York, 1988) and the references therein.
- [13] B. Rossi, *High-Energy Particles*, (Prentice-Hall, Inc. Englewood Cliffs, New Jersey, 1952)
- [14] H. W. Koch and J. W. Motz, *Rev. Mod. Phys.* **31**, 920 (1959).
- [15] W. Heitler, *The Quantum Theory of Radiation*, (Oxford Univ. Press, Oxford 1954) p194.
- [16] J. D. Bjorken and S. D. Drell, *Relativistic Quantum Mechanics*, (McGraw-Hill, New York, 1953) p133.
- [17] H.A. Bethe and J. Ashkin, *Experimental Nuclear Physics*, (John Wiley, New York, 1964) Vol. I, p166-357.
- [18] A. C. Melissinos, *Experiments in Modern Physics* p150 and p252.
- [19] This optimal condition does not allow the Fourier decomposition of Abel's integral equation as was carried out by Cormack. Hence Comack's analysis is not valid for an optimal condition of radiography.
- [20] A. B. Migdal, *Phys. Rev.* **103**, 1811 (1956).
- [21] J. W. Motz, H. A. Olsen, and H. W. Koch, *Rev. Mod. Phys.* **69**, 581(1969).
- [22] Walter R. Nelson, Hideo Hirayama, and David W. O. Rogers, *The EGS4 Code System*(SLAC Report-265, 1985).
- [23] J. O. Hirschfelder, J. J. Magee, and M. H. Hull, *Phys. Rev.* **73**, 852(1948).
- [24] J. O. Hirschfelder and E. N. Adams II, *Phys. Rev.* **73**, 863 (1948).
- [25] U. Fano, *Phys. Rev.* **76**, 739 (1949).
- [26] G. C. Wick, *Phys. Rev.* **75**, 738 (1949).
- [27] B. Rossi and K. Greisen, *Rev. Mod.* **13**, 240 (1941).
- [28] L. G. Parratt, *Phys. Rev.* **95**, 359 (1954).
- [29] P. W. Anderson, *Phys. Rev. B* **109**, 1492 (1958).
- [30] E. T. Whittaker and G. N. Watson, *A Course of Modern Analysis* (Cambridge Univ. Press, 1953) p77 and p229.
- [31] H. Jefferey and B. Jefferey, *Methods of Mthematical Analysis* (Cambridge Univ. Press, 1953) p288.
- [32] P. R. Karr and J. C. Lamkin, *Phys. Rev.* **76**, 1843 (1949).
- [33] L. V. Spencer and F. Jenkins, *Phys. Rev.* **76**, 1885 (1949).
- [34] U. Fano, H. Hurwitz, Jr. and L. V. Spencer, *Phys. Rev.* **77**, 425 (1950).

- [35] Y. S. Tsai, Rev. Mod. Phys. **46**, 815 (1974).
- [36] M. Alvada and A. Lagendijk, Phys. Rev. Lett. **55**, 2692 (1985).
- [37] P. E. Wolf and G. Maret, Phys. Rev. Lett. **55**, 2696 (1985).
- [38] This assumption is critical to the derivation of Abel's inversion (CAT scan). Hence the three dimensional CAT scan is feasible only if a test object is rotated with sufficiently small angular resolution or the x-ray source is rotated about the axis of symmetry. One may apply the Fourier decomposition with N-different views, since each view provides a one dimensional density profile as shown below.
- [39] E.T. Whittaker and G. N. Watson, *A Course of Modern Analysis* (Cambridge Univ. Press, 1953) p77 and 229.
- [40] G. M. Wing, LA-UR-84-1234.
- [41] H. Jeffereys and B. Jeffereys, *Methods of Mathematical Physics* (Cambridge Univ. Press, 1953) p288.
- [42] A. Young, Phil. Mag. Trans. A, 552 (1954).
- [43] D. C. Creagh, Nucl. Inst. and Methods in Phys. Res. **A225**, 1 (1987).
- [44] S. J. Han, LA-UR-93-2146. *Stability of a Relativistic Electron Beam in a Resistive Plasma Channel*.
- [45] M. Friedman, Phys. Rev. Lett. **32**, 92 (1974).
- [46] M. Friedman, *et al.*, Phys. Rev. Lett. **63**, 2468 (1989) and references therein.
- [47] M. V. Nezlin, Plasma Physics, **10**, 337 (1968).
- [48] M. E. Rose and M. M. Shapiro, Phys. Rev. **74**, 1853 (1948).
- [49] R. W. Hamming, *Numerical Methods for Scientists and Engineers* (McGraw-Hill Book Company, Inc, 1962) Chapter 22.

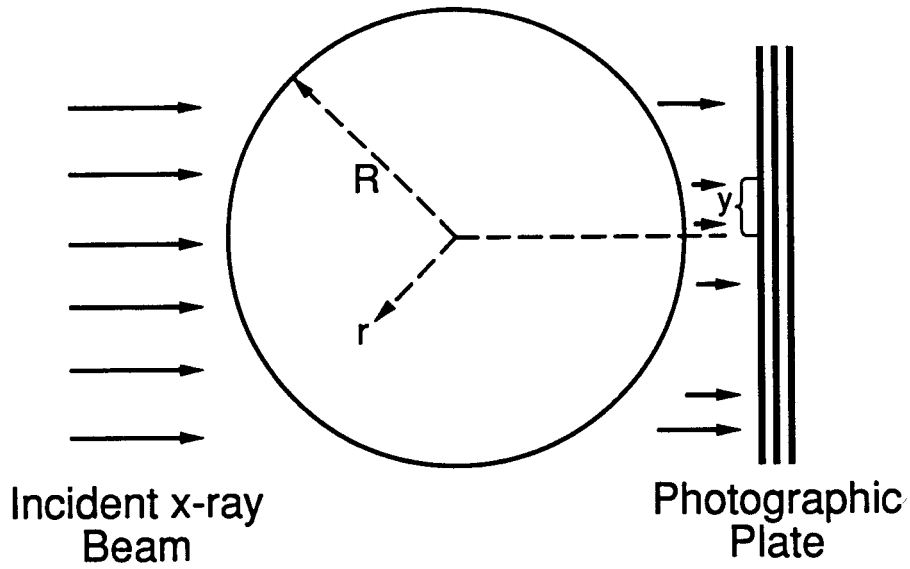


FIG. 1: A schematic picture of x-ray transmission experiments. The incident x-ray beam is approximated to be parallel uniform by the assumption that the source is very far from the test objects.

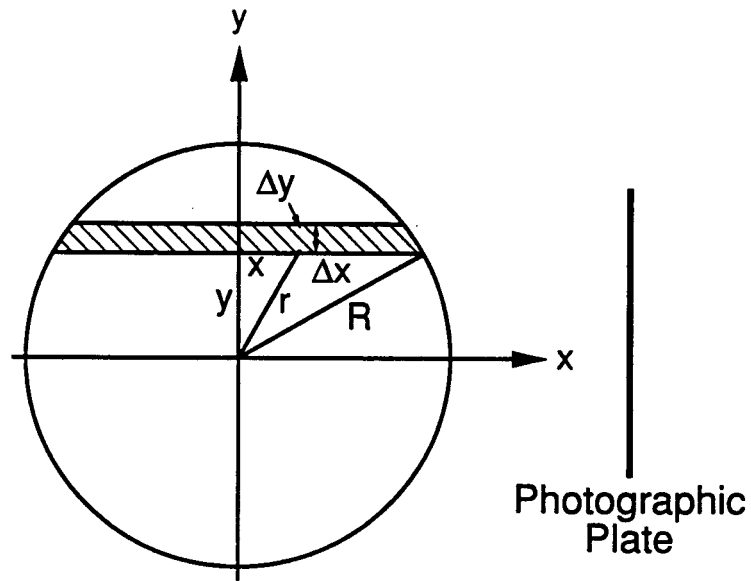


FIG. 2: The coordinate system for x-ray transmission measurements. x is the x-ray beam axis, y is the distance of a thin strip, which is parallel to the x -axis, from the center, and the cylinder is assumed to be translational invariant with respect to the z -axis.

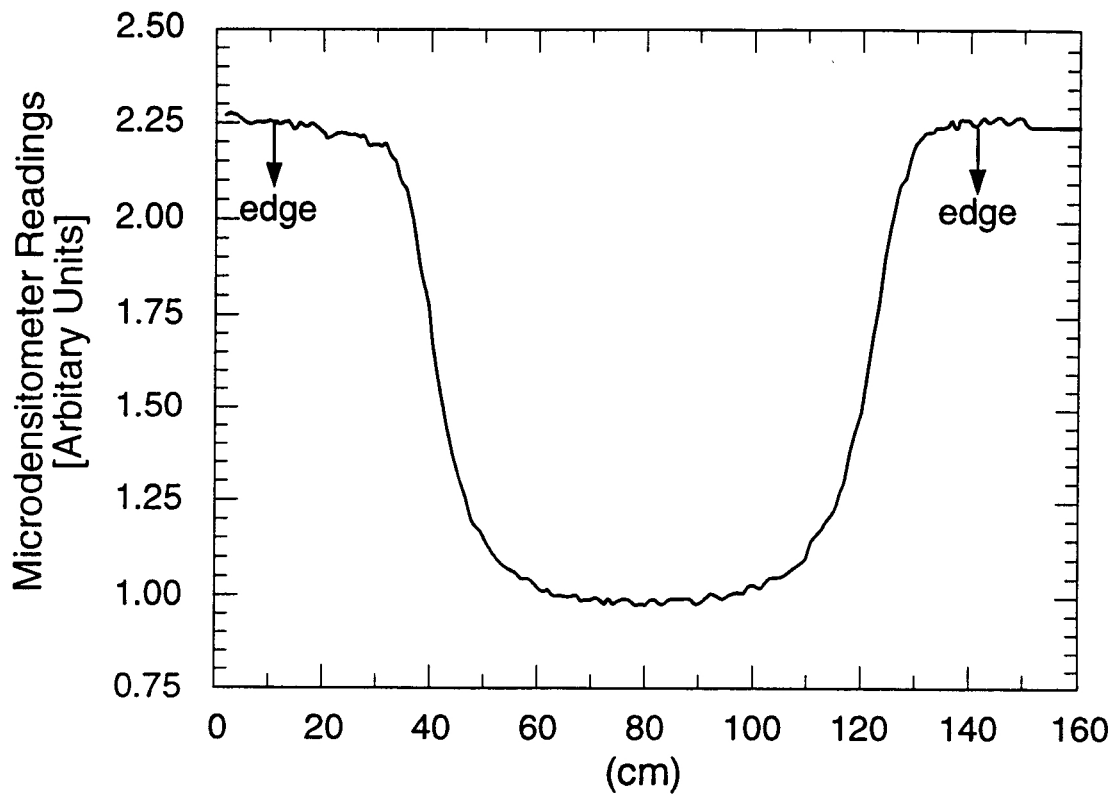


FIG. 3: A microdensitometer trace of x-ray absorption measurements for a solid U^{238} cylinder; the x-ray pulse length was approximately 15 ns.

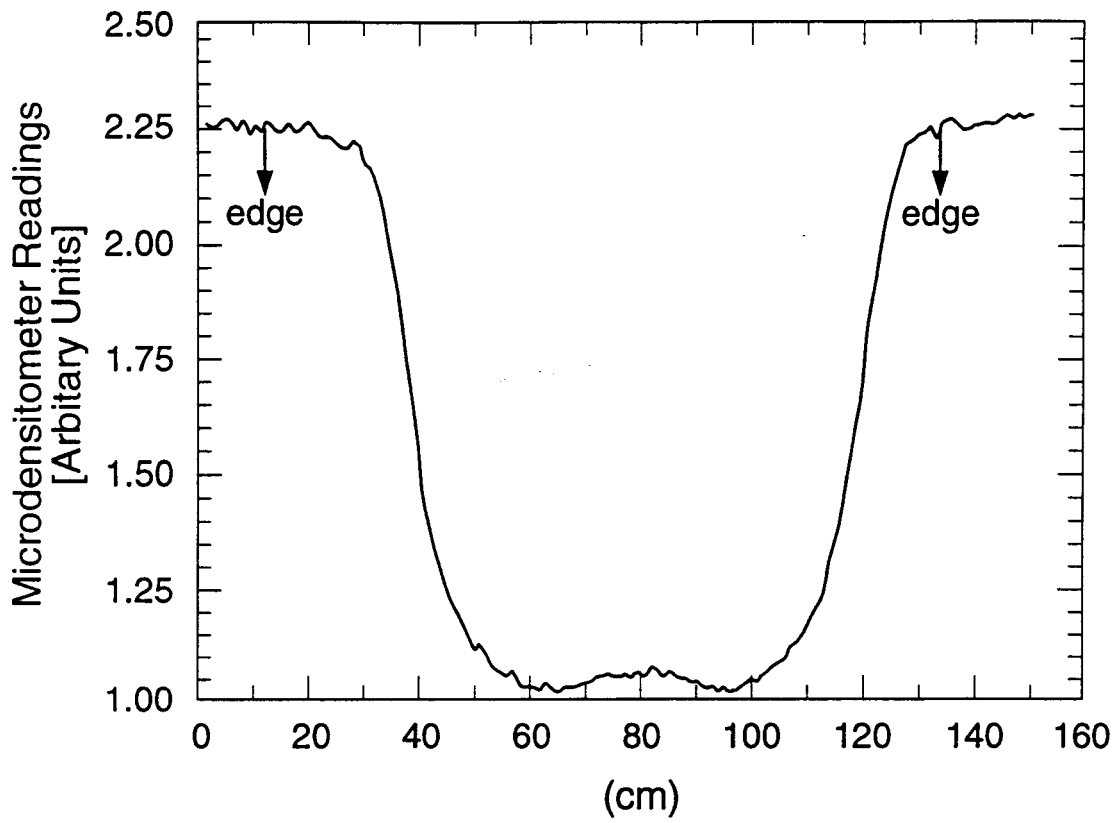


FIG. 4: A microdensitometer trace of x-ray absorption measurements for a cylindrical shell of U^{238} with the same x-ray source.

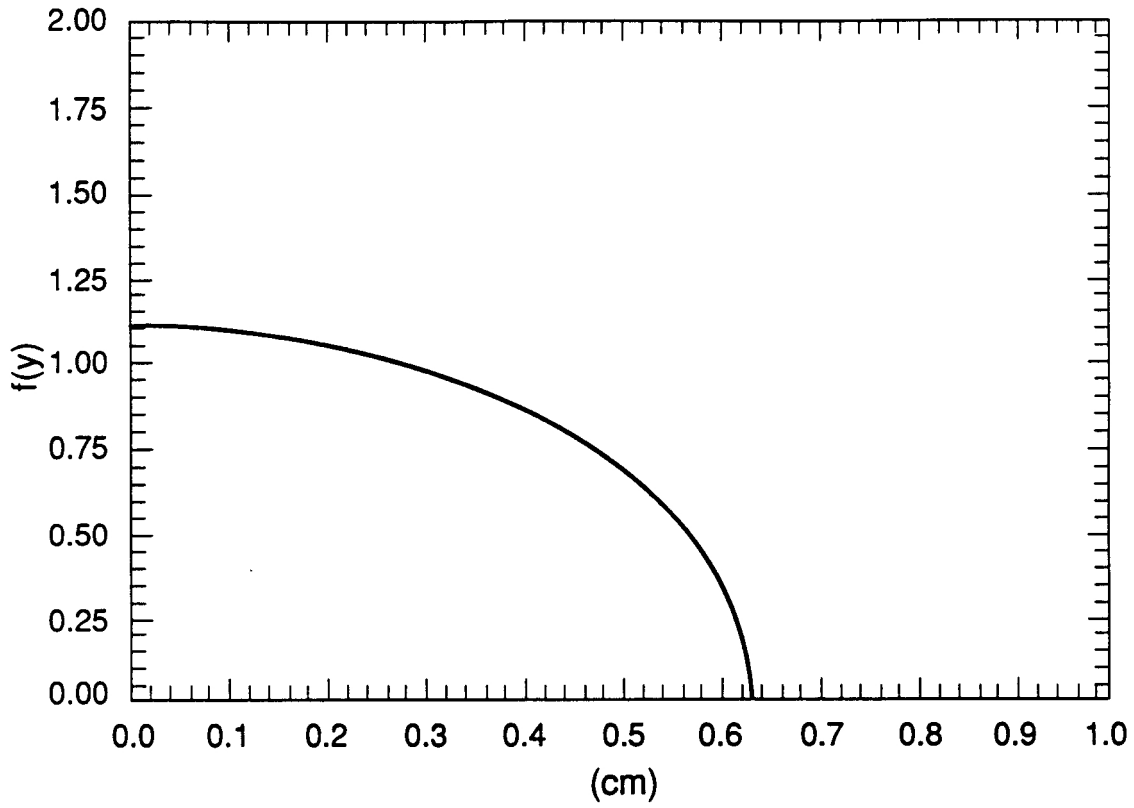


FIG. 5: The theoretically value $f(y)$ with $\mu = 0.875/cm$ for a solid cylinder. $f(y)$ was computed from Eq. (3) with $R = 0.635cm$. Note that for a constant μ , $f(y) = 2\mu(R^2 - y^2)^{1/2}$.

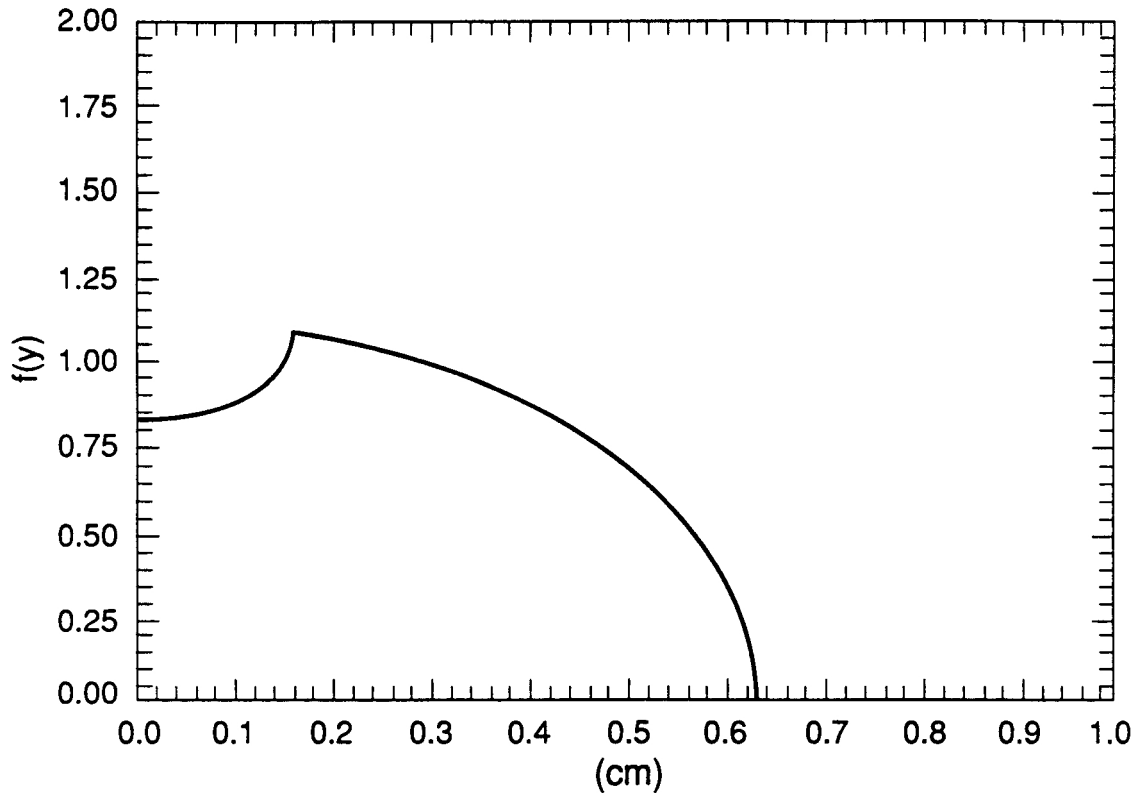


FIG. 6: The theoretically value $f(y)$ with the same $\mu = 0.875/cm$ for a cylindrical shell with $R = 0.635cm$ and $r_1 = 0.1588cm$, where R and r_1 are the outer and inner radii of the shell. For a constant μ , $f(y) = 2\mu[(R^2 - y_1^2)^{1/2} - (r^2 - y^2)^{1/2}\theta(y - r_1)]$, where $\theta(y - r_1) = 1$ for $y \geq r_1$ and $\theta(y - r_1) = 0$ for $y < r_1$.

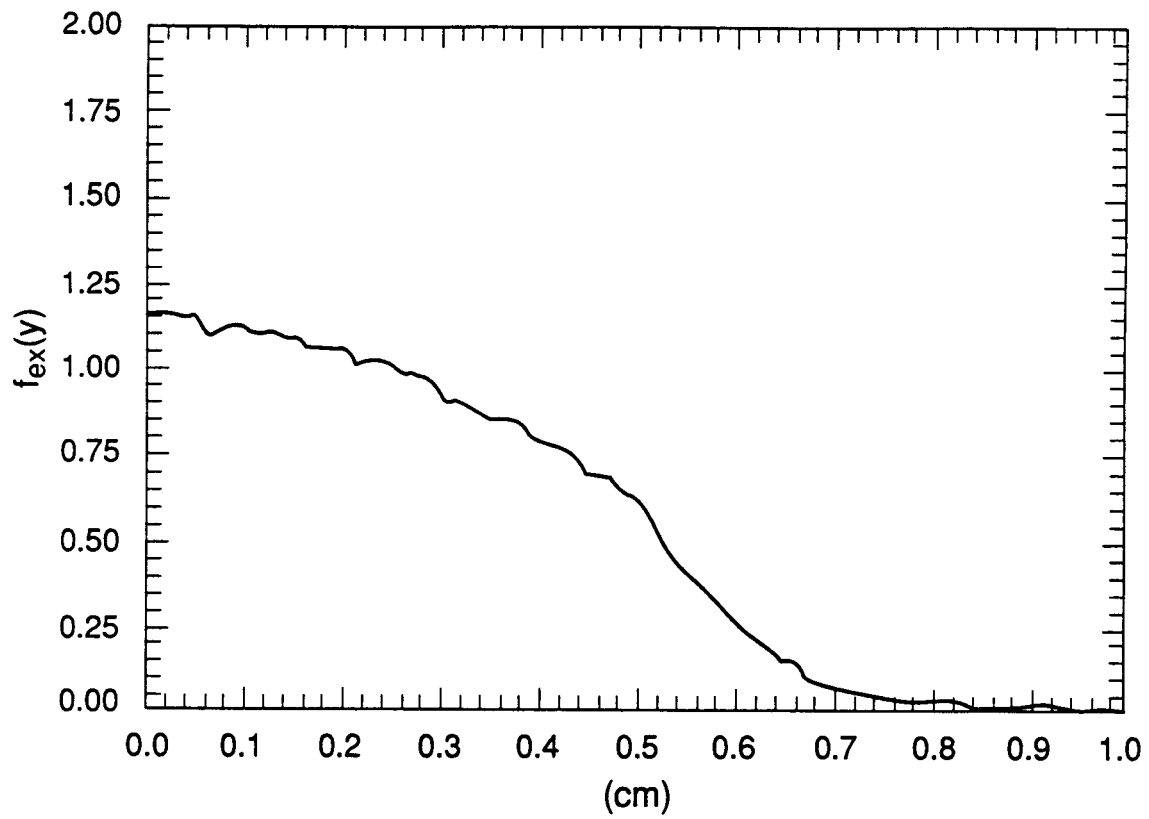


FIG. 7: The $f_{ex}(y)$ calculated from the experimental data for a solid U^{238} cylinder; it shows the intensity fluctuation and a long tail exhibiting a diffuse boundary.

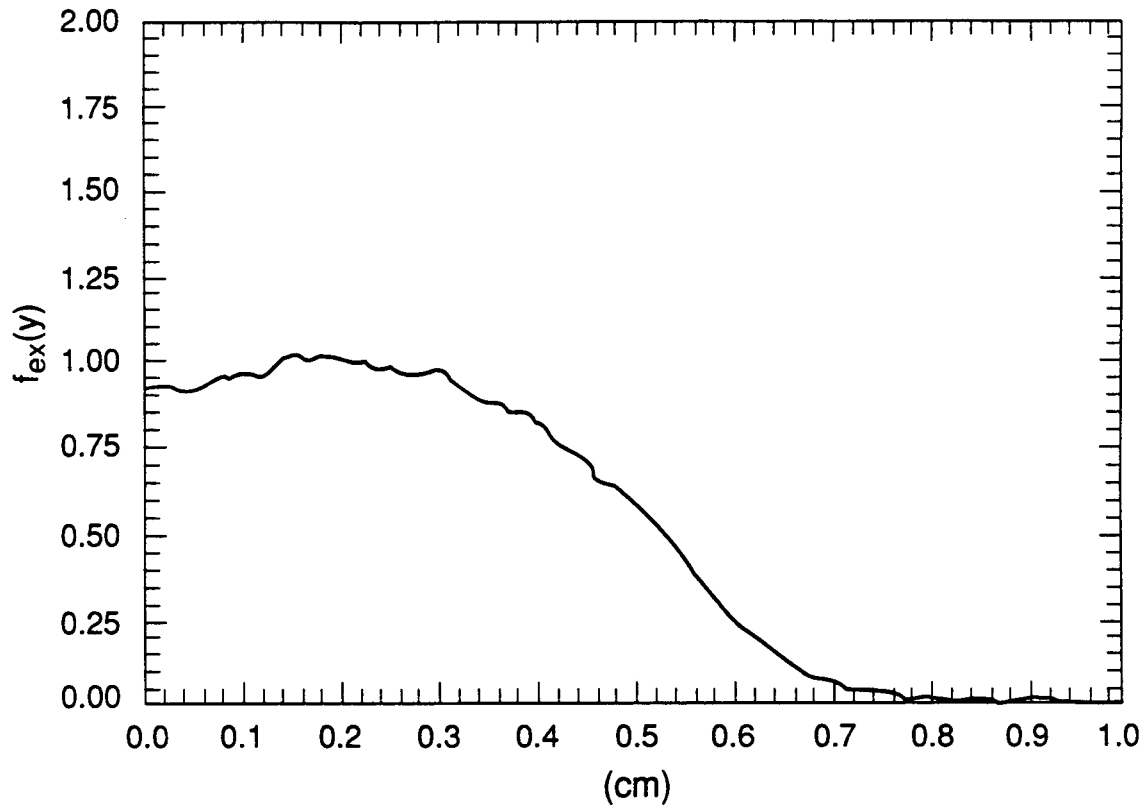


FIG. 8: The $f_{ex}(y)$ calculated from the experimental data for a hollow cylindrical (a shell) of U^{238} ; it shows an excessive x-ray absorption near the center and a long tail exhibiting a diffuse boundary.

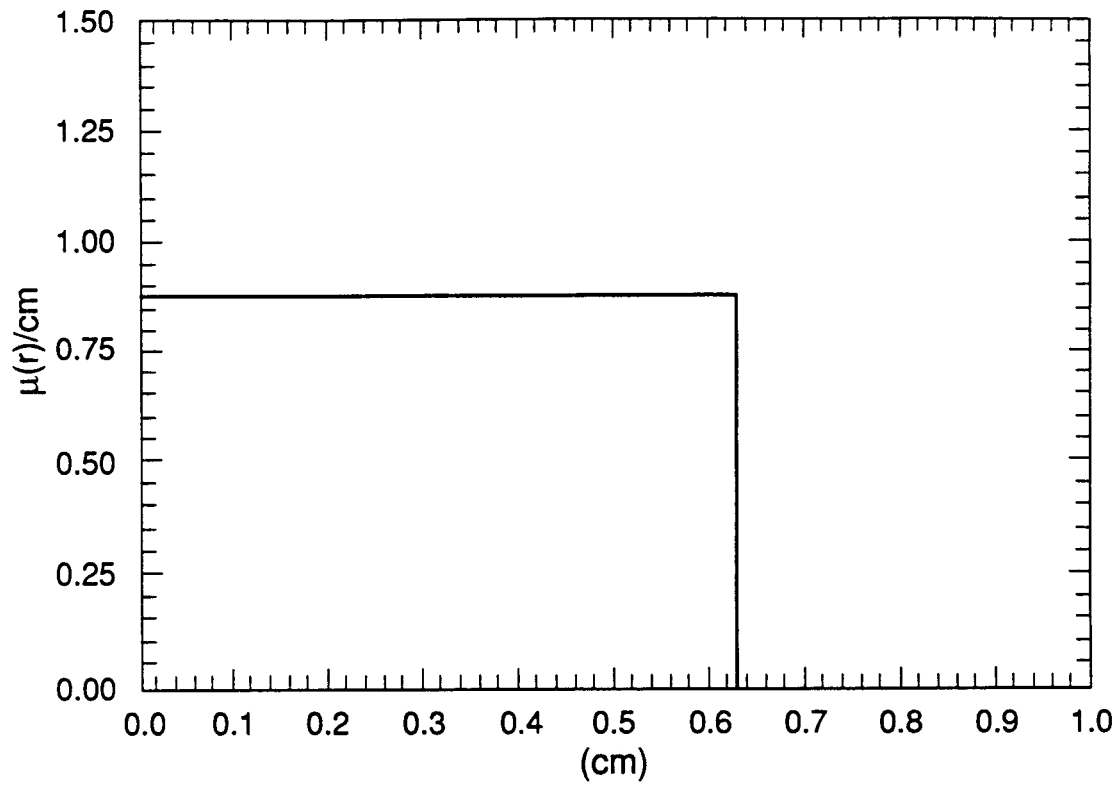


FIG. 9: The absorption coefficient calculated from Eq. (5) is shown. This demonstrates that the numerical code gives the anticipated absorption coefficient from the analytical values given in Figure 5.

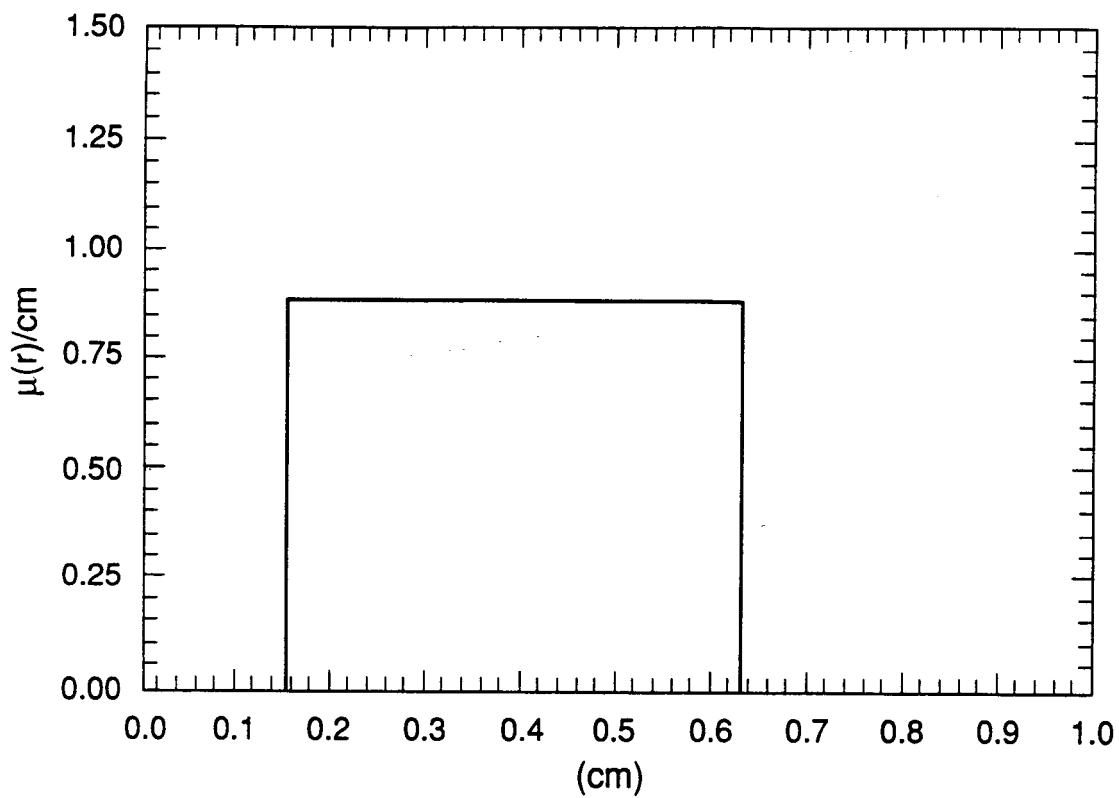


FIG. 10: The absorption coefficient computed from Eq. (5) for the solid U^{238} using the value given in Figure 6. The figure shows the code can treat a sharp boundary with little noise.

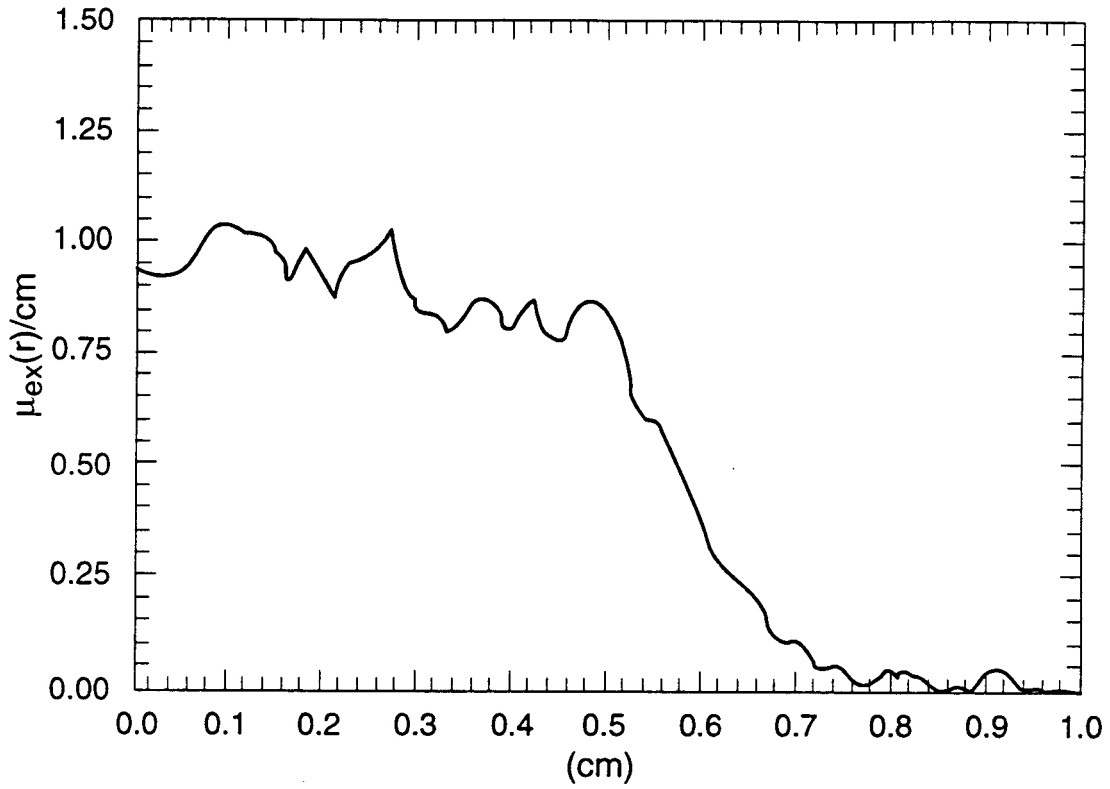


FIG. 11: The absorption coefficient computed from the experimental data on the U^{238} solid cylinder. This figure shows the x-ray intensity fluctuations due to impurities in U^{238} and a diffuse boundary. The lobes represent the interference effects of scattered x-rays with the spatially uniform incident x-rays.

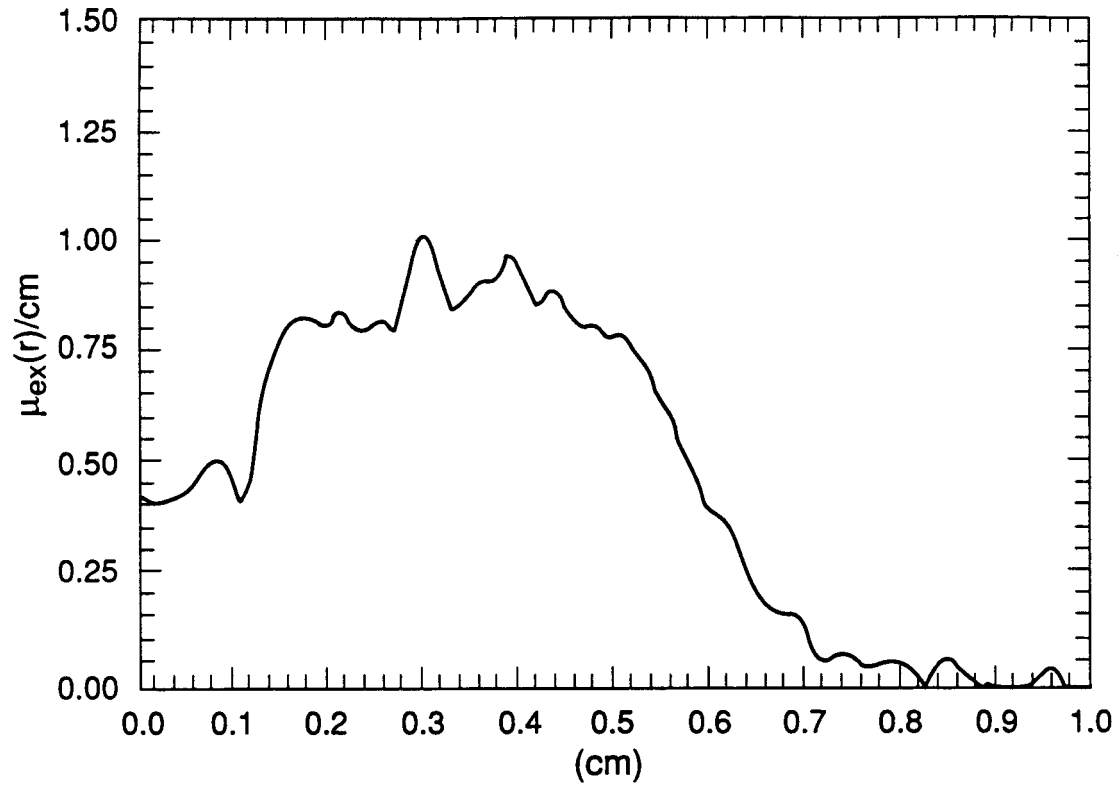


FIG. 12: The absorption coefficient computed from the experimental data on the cylindrical shell of U^{238} . The large absorption coefficient $\mu(r)$ near the center shows an excessive x-ray absorption due to the presence of a void.